Journal of Materials Chemistry C

RSC Publishing

PAPER

View Article Online
View Journal | View Issue

[*closo*-$B_{10}H_{10}$]$^{2-}$ as a structural element for quadrupolar liquid crystals: a new class of liquid crystalline NLO chromophores†‡

Cite this: *J. Mater. Chem. C*, 2013, **1**, 1144

Aleksandra Jankowiak,[a] Andrzej Baliński,[a] James E. Harvey,[a] Kristein Mason,[a] Adam Januszko,[a] Piotr Kaszyński,*[ab] Victor G. Young, Jr.[c] and Andre Persoons[d]

Received 2nd November 2012
Accepted 22nd November 2012

DOI: 10.1039/c2tc00547f

www.rsc.org/MaterialsC

Several electrically neutral, highly quadrupolar derivatives of the [*closo*-$B_{10}H_{10}$]$^{2-}$ cluster (**I**) substituted in the apical positions with onium fragments derived from 4-alkoxypyridine, 4-pentylthian, 4-pentylquinuclidine, or dinitrogen were synthesized from the parent cluster in 2–5 steps, and their thermal, structural, photophysical and dielectric properties were investigated. Only derivatives **2**, containing thianium and alkoxypyridinium substituents with linear alkyl chains, exhibit liquid crystalline behavior and form a nematic phase. α-Branching of the alkoxy chain leads to marked destabilization of both crystalline and nematic phases, which suggests the importance of polar interactions in phase stabilization of these compounds. Derivatives **2** and **3** with one π and one σ substituent, Q^+, exhibit a directional cluster-to-Q charge transfer and increase of the net electric dipole moment to $\mu_e = 17.9$ D for **2a** upon photo-excitation. They are weak fluorophores (Φ_f = 2–7%). Detailed investigation of 4-heptyloxypyridinium derivative **2b** revealed that it exhibits a nematic phase above 100 °C with $\Delta\varepsilon$ = +1.3 (130 °C), and a moderate negative solvatochromism. Hyper-Rayleigh scattering measurement gave $\beta^{HRS} = 45 \pm 10 \times 10^{-30}$ esu at 1064 nm. In solutions, and presumably in the melt, it exists as a mixture of interconverting *trans* and *cis* isomers at about 4 : 1 ratio with $\Delta G_{298} = 0.82 \pm 0.06$ kcal mol^{-1} and $\Delta G^{\ddagger}_{298} = 25.3 \pm 0.6$ kcal mol^{-1} established by VT NMR methods.

Introduction

Despite a large number of liquid crystalline materials characterized to date,[1] there are relatively few mesogenic betaines,[2–6] and quadrupolar bis-betaine mesogens are practically unknown. Such compounds are of interest for studying of fundamental and applied aspects of liquid crystals. For instance, using betaines derived from [*closo*-1-CB_9H_{10}]$^-$, we have demonstrated the effect of molecular dipole moment on phase stability,[3] and prepared high $\Delta\varepsilon$ nematic materials, including one with a record high dielectric anisotropy $\Delta\varepsilon$ = 113.[3,4] Properly designed bis-betaines derived from the isoelectronic *closo*-decaborate dianion, [*closo*-$B_{10}H_{10}$]$^{2-}$ (**I**, Fig. 1), could yield other information on the effect of polarity on phase stability,[3] and materials exhibiting useful photophysical properties, such as NLO.[7,8]

Decaborate dianion, [*closo*-$B_{10}H_{10}$]$^{2-}$ (**I**), is a 3-dimensional polarizable,[9] σ-aromatic system[10,11] with the D_{4d} molecular symmetry.[12] Its FMOs are doubly degenerated with E_1 (HOMO) and E_3 (LUMO) symmetry, and the calculated HOMO–LOMO gap of 12.96 eV (HF/6-31G*).[13,14] Consequently, the anion is transparent above 200 nm. The orbital symmetry allows for efficient electronic interactions between [*closo*-$B_{10}H_{10}$]$^{2-}$ and π substituents,[15] and intense cage-to-substituent CT bands have been observed in pyridine,[16,17] dinitrogen[13,17] and other derivatives.[18,19]

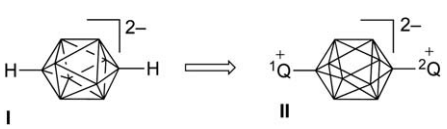

I II

Fig. 1 [*closo*-$B_{10}H_{10}$]$^{2-}$ anion (**I**) and its derivative **II**. Each unsubstituted vertex corresponds to the BH fragment. Groups $^1Q^+$ and $^2Q^+$ are onium substituents such as ammonium, sulfonium or pyridinium.

[a]*Organic Materials Research Group, Department of Chemistry, Vanderbilt University, Nashville, TN 37235, USA*

[b]*Faculty of Chemistry, University of Łódź, Tamka 12, 91403 Łódź, Poland*

[c]*X-ray Crystallographic Laboratory, Department of Chemistry, University of Minnesota, Twin Cities, MN 55455, USA*

[d]*Department of Chemistry, University of Leuven, Celestijnenlaan 200D, 3001 Leuven, Belgium*

† In part described in J. E. Harvey, III, M.Sc. Thesis, Vanderbilt University, 1999.

‡ Electronic supplementary information (ESI) available: Synthetic details and characterization and additional data for compounds **1**, **2b**, **6[NMe$_4$]**, **7a[NMe$_4$]**, **7b[NMe$_4$]**, **10a–e**, and **13**, computational details, thermodynamic and kinetic data for **2b**, details of fluorescence quantum yield measurements, experimental and theoretical solvatochromic data, details of Maier–Meier analysis, crystal structure data for **2b**, **8a** and **8b**, archive of calculated equilibrium geometries for **2b-*trans***, **2b-*cis***, **2b-TS**, **3b**, **8a–f**, and **16–21**. CCDC 875509, 875508 and 875507. For ESI and crystallographic data in CIF or other electronic format see DOI: 10.1039/c2tc00547f

Substitution of the $[closo\text{-}B_{10}H_{10}]^{2-}$ cluster (**I**) with two onium fragments, $^1Q^+$ and $^2Q^+$, at the apical positions (Fig. 1) leads to electrically neutral bis-betaines **II** with a large linear quadrupole and a small net ground state dipole moment μ_g, whose exact value depends on the nature of the onium groups. Several such parent compounds have been known,[17,20,21] including two mesogenic bis-betaines **II** reported by us.[16] The symmetric bis-pyridinium derivative **1** forms a nematic phase, exhibits a strong absorption band at 319 nm ascribed to cluster-to-ring CT, and photoemits at 480 nm. A comparison of the nematic–isotropic transition temperature T_{NI} for **1** with that of its isosteric and isoelectronic carborane analogue demonstrated that an increase of the molecular quadrupole moment coincides with stabilization of the nematic phase by 100 K.[3] Since both pyridine rings are involved in photoexcitation of **1** at 319 nm, the ground and excited state dipole moments are similar ($\mu_g \approx \mu_e$). A directional CT in bis-betaines **II** and hence $\mu_g < \mu_e$ could be achieved with two significantly different onium fragments, such as one of π type and the other of σ type. According to our previous calculations,[13,22] the net molecular dipole moment in such unsymmetrical derivatives **II** markedly increases upon excitation ($\mu_g \ll \mu_e$) due to vanishing only one of the local dipole moments, and the chromophores are expected to exhibit moderate second-order NLO properties. Quadrupolar NLO chromophores have the advantage over dipolar materials, in which $\mu_g \gg \mu_e$, because their low μ_g is more conducive to alignment of the molecules and higher stability of the requisite non-centrosymmetric material.[23] Earlier we described an unsymmetric nematic bis-betaine belonging to series **2** with a 4-heptyloxypyridine substituent **2b**,[16] and found that in a planar cell it forms a nematic glass that generates a weak SHG signal.[24] This discovery provided a further impetus for investigation of this type of mesogenic materials.

Here we provide full synthetic details and also thermal, dielectric, structural and dynamic characterizations of **2b**. Compounds **2a**, **2b**, **3b**, and two intermediates are characterized for their photophysical properties. Experimental results are compared to DFT calculations. We investigate the effect of the chain-length (**2a–c**) and branching of the alkoxy chain (**2d** and **2e**) on mesogenic properties. We analyzed the effect of replacement of the sulfonium fragment with quinuclidinium, and we characterize derivatives **3b** and **3e**. Finally, we characterize symmetric bis-betains, bis-sulfonium **4** and bis-quinuclidinium **5**.

Results

Synthesis

The preparation of hetero-disubstituted *closo*-decaborane derivatives **II** involves a sequential introduction of the onium fragments $^1Q^+$ and $^2Q^+$ at the apical positions of the $\{closo\text{-}B_{10}\}$ cluster. The strategy takes advantage of a general method for selective preparation of monodinitrogen derivatives[21] and substitution of the apical N_2^+ group with nucleophiles[17,20,21] (Fig. 2). The sequence of reactions from **6** through **7** to **8** was run without rigorous purification of the intermediate salt **7**. The non-ionic compounds **8** were obtained in moderate overall yields, rigorously purified, and fully characterized.

The monodinitrogen salt **6[NMe$_4$]** was conveniently prepared according to the original procedure for a diazo-transfer reaction from arenediazonium to $[closo\text{-}B_{10}H_{10}]^{2-}$ (Scheme 1).[21] Subsequent thermolysis of **6[NMe$_4$]** in Me_2NCHS gave the masked mercapto derivative **7a[NMe$_4$]**,[25] which was a precursor to series **2**. Thermolysis of **6[NMe$_4$]** in the presence of dry NH_3 gave ammonium derivative **7b[NMe$_4$]**, a precursor to series **3**. This method represents a convenient alternative to the reported method for the preparation of **7b[NMe$_4$]**.[18]

Synthesis of series 2. The formation of the thiane ring in **7c[NMe$_4$]** was accomplished by alkylative cyclization of the masked mercaptan **7a[NMe$_4$]** with dibromide **9** (ref. 26) under hydrolytic conditions[5,27] in the presence of $NMe_4^+OH^-\cdot 5H_2O$ (Scheme 2). The resulting salt **7c[NMe$_4$]** was diazotized using HNO_2 followed by treatment with zinc powder, according to a general method.[20] The dinitrogen intermediate **8a** was isolated in about 40–55% yield. Preparation of **8a** using the tribromobenzenediazonium salt following a general procedure[21] gave significantly lower yields, about 25%, of a yellow product, that was difficult to purify. ^{13}C NMR spectroscopy of **8a** demonstrated the presence of two isomers at approximately 4 : 1 ratio. Thermolysis of dinitrogen derivative **8a** in 4-alkoxypyridine (**10**) at 120 °C gave the sulfonium derivatives **2**.

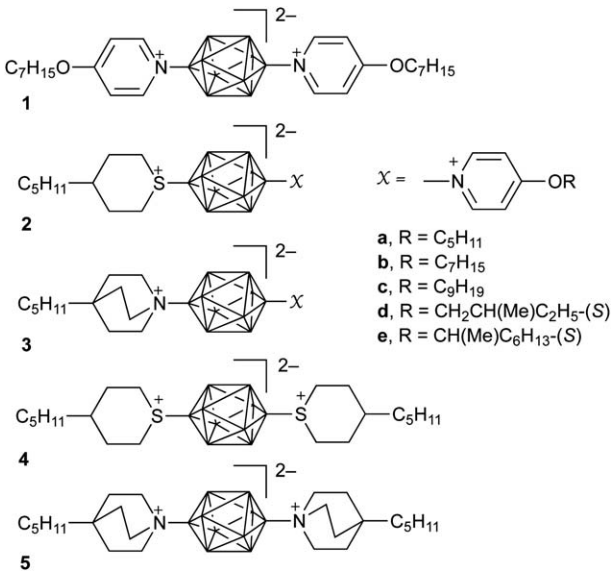

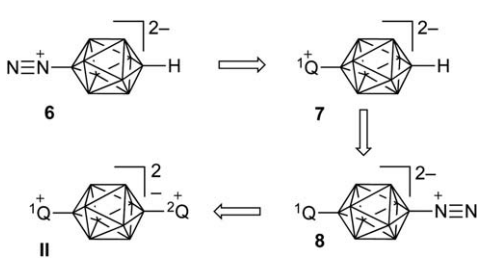

Fig. 2 General synthetic scheme for the preparation of hetero-disubstituted bis-betains **II**.

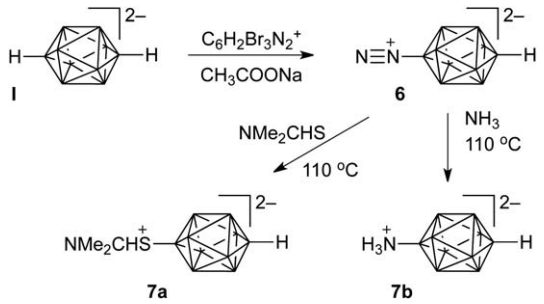

Scheme 1

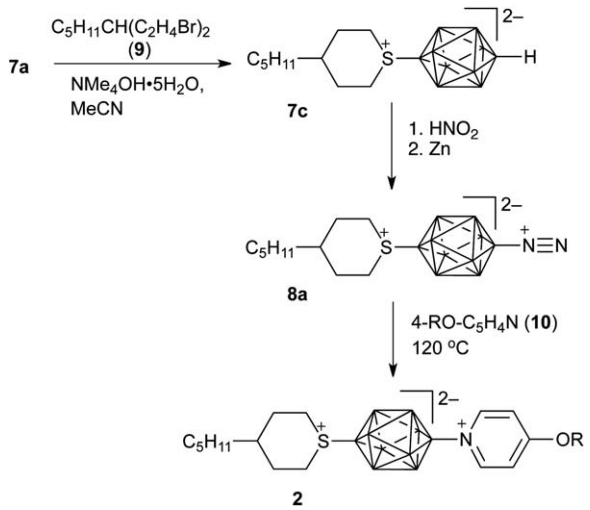

Scheme 2

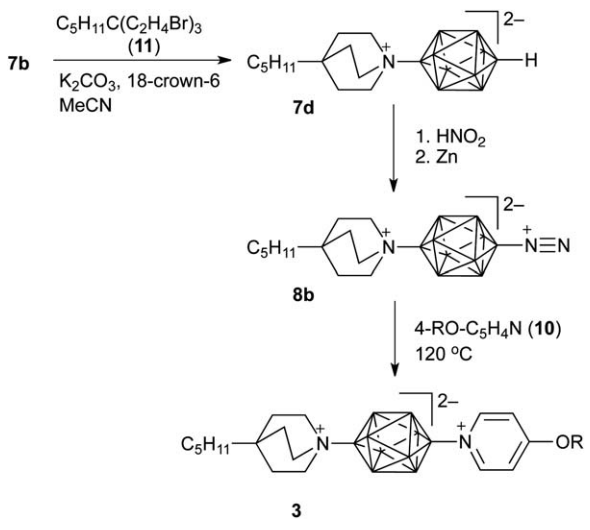

Scheme 3

Synthesis of series 3. The quinuclidine ring in derivatives **3** was constructed by alkylative cyclization of amine **7b[NMe_4]** with tribromide **11** (ref. 28) following our method reported earlier (Scheme 3).[29] Without purification, crude **7d** was substituted with dinitrogen following a general literature procedure[20] to form 1-dinitrogen derivative **8b** in 40% overall yield based on starting **6[NMe_4]**. Thermolysis of dinitrogen derivative **8b** in 4-alkoxypyridine (**10**) at 120 °C gave the pyridinium derivatives **3**.

The bis-quinuclidinium **5** was prepared in an analogous manner starting from 1,10-bis-dinitrogen derivative [*closo*-$B_{10}H_8$-1,10-$(N_2)_2$] (**12**).[17] Thermolysis of **12** in NH_3 gave the bis-ammonium derivative [*closo*-$B_{10}H_8$-1,10-$(NH_3)_2$] (**13**),[17] which upon treatment with tribromide **11** in the presence of a base gave the bis-quinuclidine derivative **5** (Scheme 4). Similarly, thermolysis of **12** in 4-pentylthian[26] (**14**) gave bis-sulfonium derivative **4** in 18% yield (Scheme 4).

4-Alkoxypyridines **10** were conveniently prepared by a reaction of 4-chloropyridine with sodium alkoxide in DMSO (Scheme 5).[30]

Chemical and thermal stability

The chemical and thermal stabilities of compounds in series **2** were tested using samples of **2b**. The pyridinium derivative **2b** was found to be stable in anhydrous solvents, and it could be recrystallized from alcohol. However, a solid sample of **2b** kept under ambient conditions, exposed to light and moisture, underwent decomposition to the extent of 10–15% after several days, and up to 40% after a year. Minimal decomposition was observed when compound **2b** was kept in the dark and under dry Ar.

The structure of the decomposition product of **2b** is unclear. The $\{B_{10}\}$ cage lacks symmetry, as is evident from the ^{11}B NMR spectrum. The most downfield signals of the pyridine ring are shifted upfield by 0.9 ppm. Mass spectrum is consistent with the incorporation of an oxygen atom to the molecule, however no O–H stretching absorption was found in the infrared spectrum of the product.

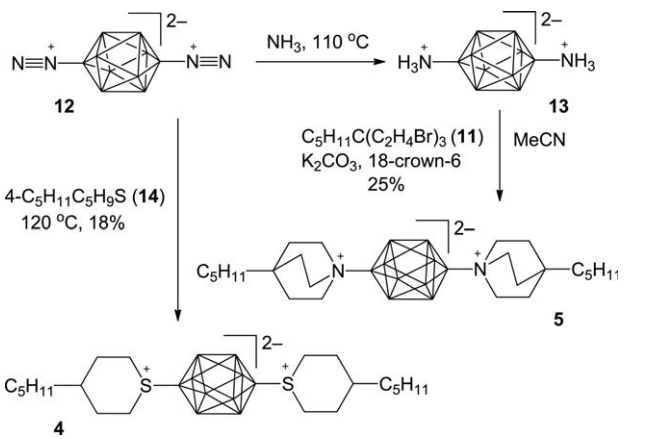

Scheme 4

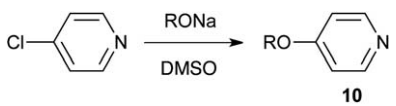

Scheme 5

Compound **2b** was also tested for thermal stability. No changes were observed in ^{1}H and ^{11}B NMR spectra after heating a neat sample of **2b** at 160 °C for 6 h under Ar. The DSC trace was practically unaffected by heating another sample of **2b** at 180 °C for 2 h.

Thermal analysis of quinuclidinium derivative **3b** demonstrated that it undergoes a partial decomposition at 280 °C, while bis-quinuclidinium **5** melts above 360 °C with complete decomposition.

Liquid crystalline properties

Transition temperatures and associated enthalpies for compounds in series **2–5** were determined by differential scanning calorimetry (DSC) and the results are shown in Table 1. Phases were identified by microscopic textures observed in polarized light.

Among all derivatives reported here, only four containing the pyridinium ring exhibit mesogenic behavior. This includes bis-pyridinium derivative **1** (ref. 16) and three derivatives **2a–c** containing the sulfonium ring. Compound **2b**, with the heptyloxypyridinium substituent, exhibits a relatively broad-range enantiotropic nematic phase with the T_{NI} of 160 °C (Fig. 3). Surprisingly, substituting a methyl group in the α position of the heptyl chain in **2b** to form chiral (*S*)-1-methylheptyl derivative **2e** eliminates the mesogenic behavior and dramatically lowers the melting point by >90 K. Extending of the heptyl chain in **2b** by 2 carbon atoms to C_9H_{19} in **2c** has marginal effect on liquid crystalline properties, however both phase transitions are lower by 6 K. On the other hand, shortening of the heptyl chain in **2b** by 2 carbon atoms to C_5H_{11} in **2a** markedly increases the melting point by 62 K with little impact on the N–I transition temperature (Table 1). Surprisingly, the chiral isomer of **2a**, containing the (*S*)-2-methylbutyl substituent (**2d**), has even higher melting point and no mesogenic behavior, even upon cooling by about 25 K below melting.

Replacement of the sulfonium ring in **2b** with quinuclidinium in **3b** increases the melting point by 161 K and eliminates mesogenic behavior. Substitution of a methyl group into the heptyl ring in **3b** only moderately lowers the melting point (by 19 K), but no mesophase was detected even upon supercooling. Replacement of the pyridinium ring in series **3** with quinuclidinium leads to a further increase of the melting point by about 100 K to over 360 °C in bis-quinuclidinium **5**. In contrast, the melting point of bis-sulfonium analogue **4** is lower by about 170 K relative to **5** and by at least 75 K relative to its longer non-mesogenic analogue **15**.[16]

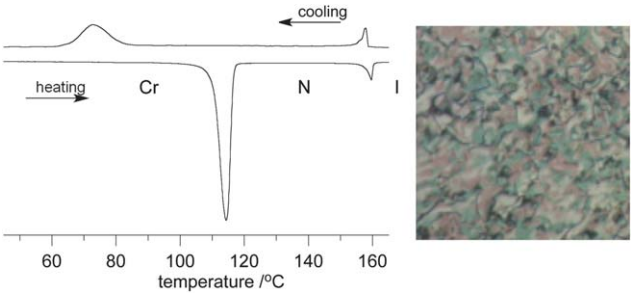

Fig. 3 DSC traces for **2b**. First heating at a rate of 4 K min^{-1}. On the right a photomicrograph of the nematic texture.

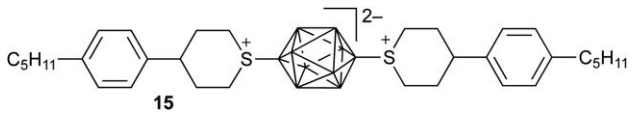

15

Table 1 Transition temperatures [°C] and enthalpies [kJ mol^{-1}] for selected compounds[a]

Compound	Cr	N	I
1[b]	• 205 (3.8)	• 225 (0.2)	•
2a, R = C_5H_{11}	• 176 (17.8)[c]	(• 162)[d]	•
2b, R = C_7H_{15}	• 114 (24.5)	• 160 (0.9)	•
2c, R = C_9H_{19}	• 108 (25.1)	• 154 (1.1)	•
2d, R = $CH_2CH(Me)C_2H_5$	• 201 (25.6)		•
2e, R = $CH(Me)C_6H_{13}$	• <25		•
3b R = C_7H_{15}	• 285[e,f]		•
3e, R = $CH(Me)C_6H_{13}$	• 266 (28.3)[f]		•
4	• 195 (28.3)		•
5	• 364 (31.0)[f]		•

[a] Observed phases are denoted by bullets and transition enthalpies are in parentheses. Cr-crystal, N-nematic, I-isotropic. [b] Ref. 16. [c] Cr–Cr transition at 128 (8.0 kJ mol^{-1}). [d] Monotropic transition established by microscopy. [e] Cr–Cr transition at 153 (13.9 kJ mol^{-1}). [f] Partial decomposition.

Molecular and crystal structures

Colorless, monoclinic crystals of **2b** and **8a**, and triclinic crystals of **8b** were grown from a CH_2Cl_2–hexane mixture by slow evaporation. Their solid-state structures were determined by X-ray diffraction[31] and pertinent interatomic dimensions are shown in Fig. 4 and Table 2.

Crystallographic analysis of a single crystal of **2b** revealed two molecules, both *trans* isomers (Fig. 4), in the asymmetric unit cell, which constitute about 80% of the sample. The remaining material was disordered and not refined. In both molecules, the thian ring adopts a nearly ideal chair conformation, while the pyridine ring is essentially planar and has a staggered orientation relative to the borane cluster. The pentyl chain adopts the gauche conformation with the dihedral angle of 70.4(8)° in molecule A of **2b**, while in molecule B the pentyl chain is disordered at a 0.62 : 0.38 ratio. In contrast, the heptyl chain was found in all-*trans* conformation and approximately co-planar with the pyridine ring in both molecules. The total length of the rigid core is about 12.5 Å, and the whole molecule 27.7 Å.

The dinitrogen derivative **8a** also contains two unique molecules of the *trans* isomer in the asymmetric unit cell. No positional disorder was found and the pentyl chain adopts all-*trans* conformation in both molecules (Fig. 4).

There is only one unique molecule in the unit cell of quinuclidine derivative **8b**. Analysis demonstrated that the quinuclidine ring is slightly twisted by 2.7° (avg.) and has smaller cylinder of rotation than that of the {*closo*-B_{10}} cluster (4.14 Å *vs.*

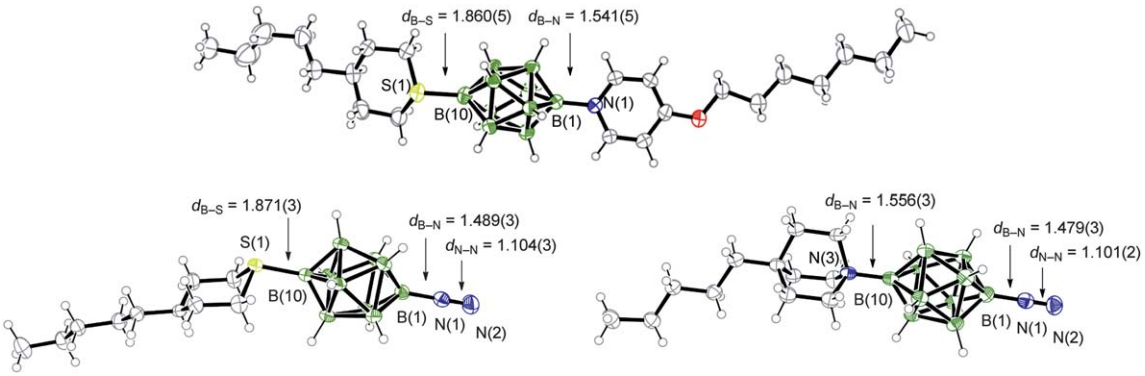

Fig. 4 Thermal ellipsoid diagram representations of **2b** (molecule A), and dinitrogen intermediates **8a** (molecule A) and **8b**.

4.72 Å). The total length of the rigid core in **8b** ($B(1)\cdots C(4)_{quin}$) is 7.76 Å (Fig. 4).

The B(1)–N_2 bond distance in dinitrogen derivatives **8a** (d_{B-N} = 1.486(4) Å) and **8b** (d_{B-N} = 1.479(3) Å) is similar to that found in [*closo*-$B_{10}H_9$-1-N_2]$^-$ anion[32] and 0.02 Å shorter than that reported for [*closo*-$B_{10}H_8$-1,10-$(N_2)_2$] (d_{B-N} = 1.499(2))[33] (Table 2).

The S–B distances in **2b** and **8a**, averaged for two unique molecules in each compound, are similar, 1.850(5) Å and 1.870(3) Å, respectively. They are close to d_{S-B} = 1.866(3) Å reported for [*closo*-$B_{10}H_8$-1,10-$(SMe_2)_2$],[34] and fall into a range of d_{S-B} = 1.83 Å reported[35] for anion [*closo*-$B_{10}H_9$-1-SMe_2]$^-$, and 1.89(1) Å found in ruthenium complex [*closo*-$B_{10}H_8$-1-SMe_2-10-N_2-RuL].[36] In all these derivatives the lone pair of the S atom eclipses the B–B bond. A similar S–B(10) bond length was found in a {*closo*-1-CB_9} derivative.[27]

A comparison of dinitrogen derivatives in Table 2 suggests that substitution of the [*closo*-$B_{10}H_9$-1-N_2]$^-$ anion at the B(10) position with electron withdrawing groups decreases pyramidalization at the B(10) position from 100.6° to 105.8° and the average deck-to-deck separation from 1.687 Å to 1.678 Å, which results in an overall contraction of the {*closo*-B_{10}} cage from 3.585 Å in [*closo*-$B_{10}H_9$-1-N_2]$^-$ to 3.494 Å in [*closo*-$B_{10}H_8$-1,10-$(N_2)_2$].

Table 2 Comparison of selected interatomic distances and angles for several derivatives of 1-dinitrogen-*closo*-dodecaborate(-1)

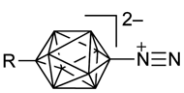

Atoms	**8b**[a] R = Quin$^+$	**8a**[a] R = Thian$^+$	R = N_2^{+b}	R = H[c]
B(1)–N_2	1.479(3)	1.486(4)	1.499(2)	1.489(6)
B(10)–R	1.5567(6)	1.870(3)	1.499(2)	1.208
B(1)–B(2–5) avrg	1.674(3)	1.677(4)	1.678(3)	1.662(7)
B(2–5)–B(6–9) avrg	1.805(4)	1.810(4)	1.799(3)	1.805(7)
B(6–9)–B(10) avrg	1.687(3)	1.682(4)	1.678(3)	1.687(7)
B–B(1)–B (avrg)	104.6(2)	104.9(2)	105.8	104.9(4)
B–B(10)–B (avrg)	101.9(2)	105.0(2)	105.8	100.6(4)
B(1)$\cdots$B(10)	3.584	3.563	3.494	3.585
N–N	1.101(2)	1.103(3)	1.091(2)	1.097(6)

[a] This study. [b] Ref. 33. [c] Ref. 32.

Molecular modeling and conformational analysis

For a better understanding of molecular and bulk properties of compounds **1–5**, their molecular geometries and electronic structures were modeled using DFT methods. Detailed comparison of equilibrium geometries obtained at the B3LYP/6-31G(d,p) level of theory with experimental bond lengths for **2b**, **8a** and **8b** revealed that the DFT method generally overestimates interatomic distances by an average of 0.011 ± 0.014 Å, with the B–B distances being reproduced most accurately.

Computational analysis of model compounds **8c–e** was used to establish conformational preference of the heterocycles relative to the {*closo*-B_{10}} cluster. The DFT calculations demonstrated that the lone pair of the sulfur atom in the thian ring eclipses the B(1)–B bond of the {*closo*-B_{10}} cluster in a conformational minimum in **8c**, while the staggered orientation of the lone pair was found in the rotational TS (Fig. 5). The quinuclidine ring in **8d** is slightly twisted ($\Theta_{N-C-C-C}$ = 8°) and adopts a pseudo-eclipsed conformation relative to the cage in the conformational minimum ($\Theta_{C-N-B(10)-B}$ = 5.6°). Similar analysis for **8e** revealed that the pyridine ring adopts an ideal staggered orientation with respect to the cage in the conformational minimum, and eclipsed in rotational TS. Analysis of the activation parameters for rotational about the X–B bond revealed a rather flat potential energy surface with the enthalpy of activation essentially 0 kcal mol^{-1} and $\Delta G^{\ddagger}_{298}$ due to entropy change (1.6 kcal mol^{-1} for **8c** and 1.9 kcal mol^{-1} for **8e**). A rotational transition state for the quinuclidine derivative could not be located.

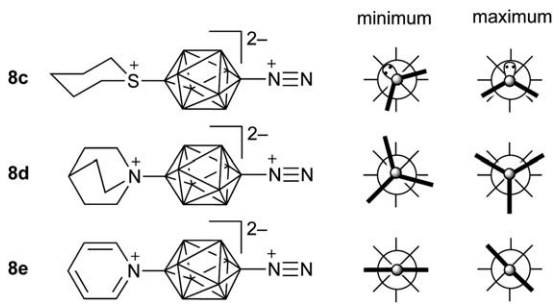

Fig. 5 Extended Newman projection along the long molecular axes of **8**. The bars represent the substituent ring and the circle is the nitrogen or sulfur atom.

The observed preferences for the orientation of the heterocyclic ring relative to the {*closo*-B_{10}} cluster are consistent with XRD results and appear to be common for all 10-vertex *closo*-boranes. The same types of conformational ground state were found for derivatives of the {*closo*-1-CB_9} cluster.[5,27]

As a consequence of the orientation of substituents in **8** relative to the D_{4d}-symmetric boron cage, all conformers for bis-pyridinium **1**, bis-sulfonium **4**, and bis-quinuclidinium **5** are chiral. In series **2** there is a conformer in which the core is C_s symmetric. This C_s symmetry of the core is lost in series **3** due to the twisted conformation of the quinuclidine ring. Considering the orientation of all-*trans* alkyl chains attached to the heterocyclic substituents, more linear ground state conformers are found for compounds in series **3** than in series **2**.

Configurational mobility

The high concentration of the isomer **2b-*trans*** in the solid sample of **2b** indicated by X-ray analysis was confirmed by low temperature NMR spectroscopy, which showed only one set of ^{1}H and ^{13}C signals for a freshly dissolved crystalline sample of **2b** in toluene-d_8 or $CDCl_3$ at −40 °C. The second set of signals belonging to the *cis* isomer slowly grew in at ambient temperature. Toluene was found to be a particularly convenient solvent for NMR analysis, since the pyridine ring ^{1}H signals were separated by approximately 16 Hz (low field signals, Fig. 6) and 8 Hz (high field signals) in the two isomers. In $CDCl_3$ these signals superimpose. Interestingly, pyridine hydrogen atoms are more shielded at lower temperature due to the change of the dielectric constant of the solvent (Fig. 6). Some of the ^{13}C signals for **2b** are well separated in both solvents.

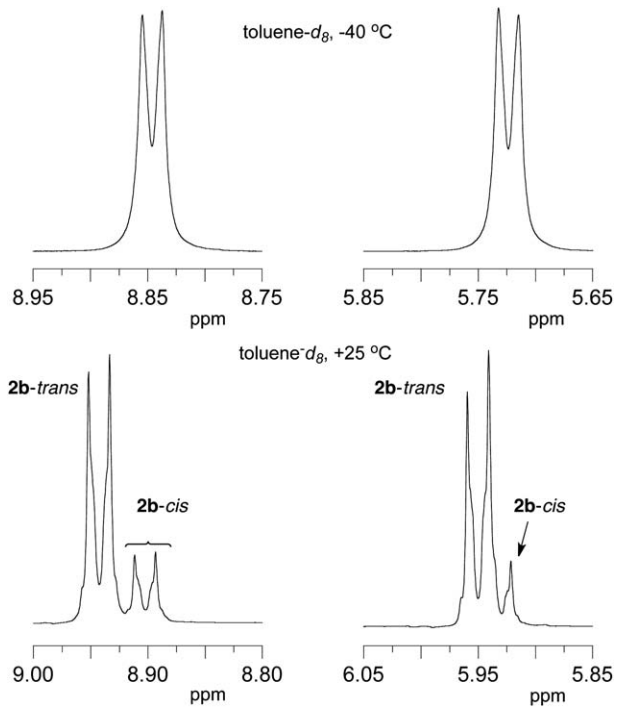

Fig. 6 Low field portion of the ^{1}H NMR spectrum of **2b** in toluene-d_8.

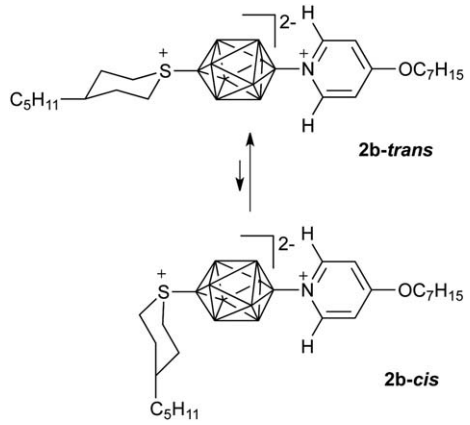

Fig. 7 Interconversion of the *trans* and *cis* isomers of **2b**. Two major conformers are shown with the diagnostic aromatic H atoms.

Sufficient separation of the low field signals in toluene was used to establish thermodynamics of the isomerization process (Fig. 7). Thus, measurements of the ratio of the signals at equilibrium in the temperature range 50–100 °C allowed us to calculate the enthalpy and entropy difference, $\Delta H = 1.06 \pm 0.06$ kcal mol^{-1} and $\Delta S = +0.82 \pm 0.06$ cal mol^{-1} K^{-1}, between the two isomers **2b-*trans*** and **2b-*cis*** shown in Fig. 7.[37] Equilibrium data extrapolated to lower temperatures were used to calculate rates for isomerization. It was found that the *trans*-to-*cis* conversion is a first-order process with rate constants $k = 8.7 \pm 0.2 \times 10^{-4}$ s^{-1} at 25 °C. Measurements in the range of 0–25 °C allowed us to calculate activation parameters, $\Delta H^{\ddagger} = 23.5 \pm 0.6$ kcal mol^{-1} and $\Delta S^{\ddagger} = -6 \pm 2$ cal mol^{-1} K^{-1} for the process.[37]

DFT calculations for **2b** in toluene dielectric medium are consistent with experimental results and show similar theoretical values for the equilibrium ($\Delta H = 1.31$ kcal mol^{-1} and $\Delta S = +0.3$ cal mol^{-1} K^{-1}) and isomerization process ($\Delta H^{\ddagger} = 20.5$ kcal mol^{-1} and $\Delta S^{\ddagger} = 6.4$ cal mol^{-1} K^{-1}).

Photophysical properties

Absorption/emission. Electronic spectra for pyridinium **2a**, **2b** and **3b**, and dinitrogen derivatives **8a** and **8b**, were recorded in MeCN and selected data are presented in Fig. 8 and Table 3.

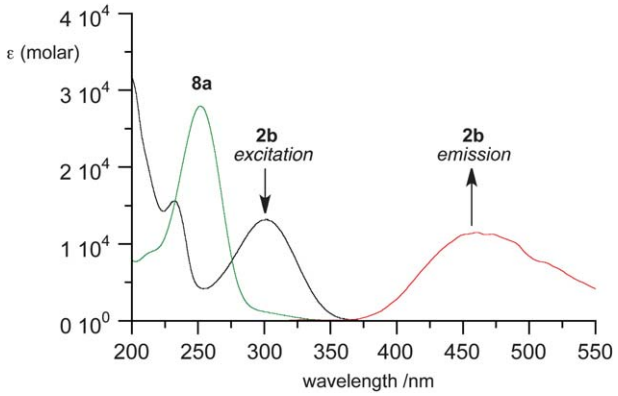

Fig. 8 Absorption spectra for **2b** and **8a** and emission spectrum for **2b** in MeCN.

Table 3 Selected experimental[a] and calculated[b] electronic transition energies and oscillator strength values

	Experimental[a]		Theoretical[b]	
	Absorption λ_{ab}/nm	Emission[c] λ_{em}/nm	Stokes shift ΔE/eV	$\pi \rightarrow \pi^*$ (f)
2a	301	466	1.46	320 (0.44)
2b	301	463	1.43	320 (0.44)
3b	310	475	1.39	332 (0.39)
8a	252	—	—	265 (0.47)
8b	255	—	—	264 (0.39)

[a] Recorded in MeCN. [b] Obtained with TD B3LYP/6-31(d,p)||B3LYP/6-31(d,p) method in MeCN dielectric medium. [c] Excitation at the wavelength of maximum absorption.

All pyridinium derivatives exhibit moderate absorption with maxima in a region of about 300 nm and 230 nm, while the absorption bands for the dinitrogen **8a** and **8b** are in a region of about 255 nm. The position of maxima for the quinuclidinium derivatives are slightly shifted to lower energies and have lower molar extinction coefficients relative to the sulfonium analogues. These findings are consistent with results of TD-DFT calculations (Table 3).

Solutions of pyridinium derivatives **2** and **3** fluoresce at ambient temperature with a substantial Stokes shift. For instance, the pentyloxy derivative **2a** has a maximum of emission at 466 nm (λ_{ex} = 301 nm), which corresponds to a Stokes shift of 1.46 eV (Table 3). Similar results were obtained for **2b** (Table 3 and Fig. 8). Comparison of compounds **2** and **3** with quinine bisulfate reference[38] demonstrated that they are inefficient fluorophores. Thus, a fluorescence quantum yield, Φ_f, of 4% and 2% was measured for **2a** and **3b**, respectively, in MeCN, while in CH_2Cl_2 Φ_f = 7% was found for **2a**. The dinitrogen compounds **8** do not fluoresce under these conditions.

TD-DFT calculations in MeCN dielectric medium indicate that the observed lowest energy absorption bands in pyridinium derivatives **2b** and **3b** involve transition from the HOMO, localized primarily on the {*closo*-B_{10}} cluster, to the LUMO, localized on the pyridine substituent, as shown for **3b** in Fig. 9. In the dinitrogen derivative **8b** excitation at about 255 nm involves nearly double degenerate MOs constituting the HOMO and HOMO-2 localized on the {*closo*-B_{10}} cage and the LUMO localized mainly on the N_2 substituent.[37] In the sulfonium derivatives such as **2b** and **8a** the orbital energies are more differentiated due to the involvement of the sulfur atom lone pair.[37]

Solvatochromism and exited state dipole moment. Low energy absorption bands in compound **2**, **3** and **8** exhibit a moderate negative solvatochromic effect, and they are shifted to higher energies with increasing solvent polarity expressed by normalized E_T^N parameter[39] (Fig. 10). The observed trend in λ_{max} was reproduced with TD-DFT calculations in dielectric media of appropriate solvents.[37] In contrast, emission bands weakly depend on solvent polarity and their energies decrease with increasing solvent polarity (small positive solvatochromic effect).

The magnitude of the Stokes shift ($\nu_{ab} - \nu_{fl}$) in **2a** was solvent dependent and was treated with the Lippert–Mataga formalism (eqn (1)) to estimate the excited state dipole moment, μ_e.[37,40] A plot of Stokes shift *vs.* solvent parameter Δf gave the slope 17.85 ± 1.6 × 10^3 cm^{-1} (Fig. 11), from which the change of the dipole moment $\Delta\mu$ = 21 ± 1 D was obtained.[37] The radius of the

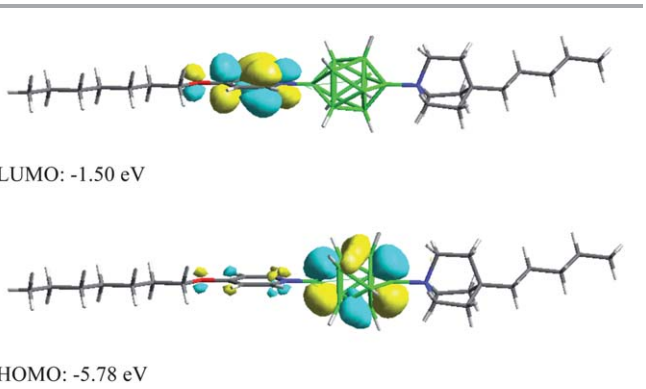

Fig. 9 B3LYP/6-31G(d,p) derived contours and energies of frontier molecular orbitals for **3b** in MeCN dielectric medium.

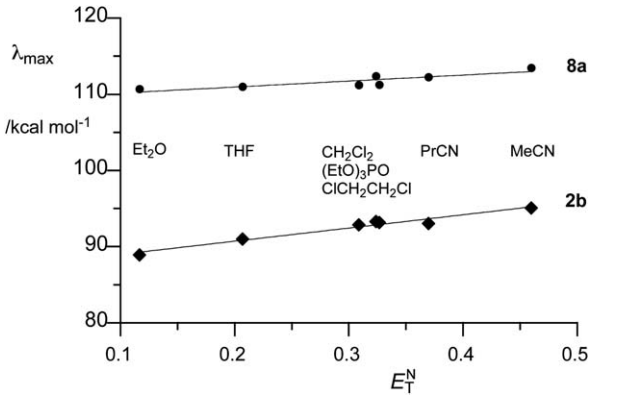

Fig. 10 Dependence of absorption energy for **2b** and **8a** on solvent polarity E_T^N. Slope: 17.3 ± 1.6, r = 0.98 (**2b**) and 7.9 ± 1.9 r = 0.88 (**3b**).

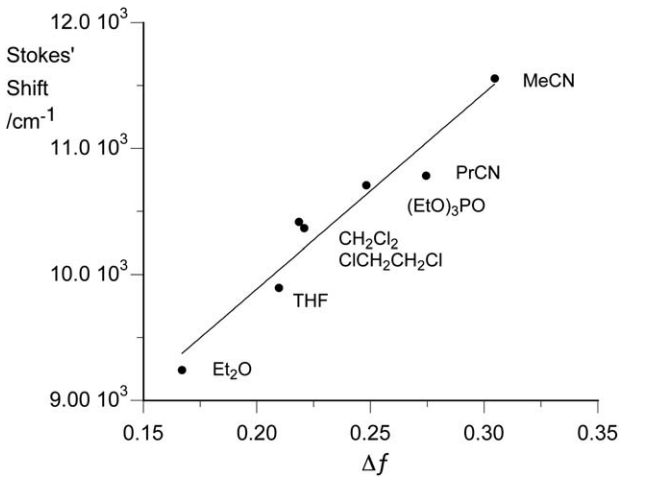

Fig. 11 Lippert–Mataga plot for **2a**: Stokes shift *vs.* solvent parameter Δf. Slope: 17.85 ± 1.6 × 10^3 cm^{-1} (r^2 = 0.963).

solvent cavity (a_0) used in eqn (1) was obtained from DFT calculations.

$$(\nu_{ab} - \nu_{fl}) = \frac{2(\mu_e - \mu_g)^2}{4\pi\varepsilon_0 hca_0^3}\Delta f + \text{const} \quad (1)$$

Analysis of the orientation and magnitude of the calculated molecular dipole moment for parent dinitrogen compounds **8c** ($\mu_g = 8.68$ D), **8d** ($\mu_g = 9.39$ D), **8e** ($\mu_g = 10.36$ D), (Fig. 5) and the 4-methoxy analogue of **8e**, derivative **8f** ($\mu_g = 12.55$ D) in CH_2Cl_2 dielectric medium indicates that the effectiveness of the substituents in inducing local dipole moment increases in the order N_2^+– < R_2S^+– < R_3N^+– < $C_5H_5N^+$– < 4-$MeOC_5H_4N^+$–. With the dipole moment contribution for the N_2^+– estimated from DFT results for two isomeric derivatives [*closo*-1-CB_9H_9-1-N_2] ($\mu_g = 7.74$ D) and [*closo*-1-CB_9H_9-10-N_2] ($\mu_g = 3.04$ D) in CH_2Cl_2 dielectric medium, absolute values for other substituents were calculated as follows: $C_5H_{10}S^+$– (14.1 D), $C_7H_{13}N^+$– (14.8 D) $C_5H_5N^+$– (15.8 D), and 4-$MeOC_5H_4N^+$– (17.9 D), assuming additivity of the local dipole moments in derivatives **8.** Using the calculated values for substituents, the ground state dipole moment for compound **16** was estimated at 3.8 D, while the DFT calculated value was 4.3 D, which represents a reasonably good agreement (Fig. 12).

Upon cluster-to-pyridine excitation, the larger of the two local dipole moments essentially vanishes leaving the smaller local dipole as the major contributor to the net molecular dipole moment μ_e of **16***. As a result the molecule becomes more polar and the change $\Delta\mu = \mu_e - \mu_g$ is 17.9 D, since the two dipoles have opposite orientation.

Results obtained for **2a** from the Lippert–Mataga analysis are consistent with this model. Thus, the dipole moment for **2a*** can be estimated at about $\mu_e = 16$ D using a DFT-computed value for **2a** of $\mu_g = 4.8$ D in CH_2Cl_2 dielectric medium.

Molecular hyperpolarizability. First hyperpolarizability $\beta_{(-\omega,\omega,0)}$ was calculated for selected molecules in CH_2Cl_2 dielectric medium at two frequencies ω with the DFT method, and compared to results for standard NLO materials such as *p*-nitroaniline[41,42] (**PNA**), 4-(*N*,*N*-dimethylamino)nitrobenzene[43] (**DMANB**), and 4-methoxy-4′-nitrostilbene[41] (**MONS**, Table 4).

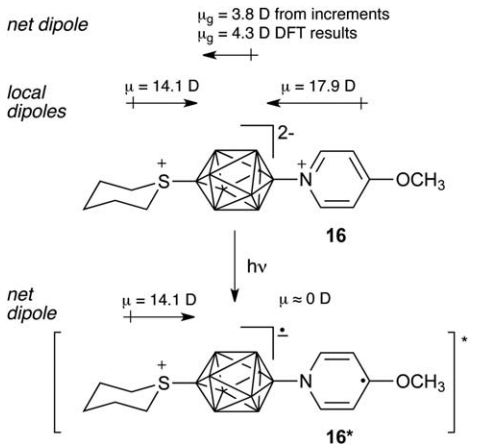

Fig. 12 Local and net dipole moments estimated for ground and excited states of **16**. For details see text.

Results demonstrate that values of the $\beta_{(-\omega,\omega,0)\|}$ calculated for {*closo*-B_{10}} derivatives are comparable with those for single-ring organic reference chromophores, and an order of magnitude lower than those obtained for stilbene **MONS**, a two-ring chromophore. Values of $\beta_{(-\omega,\omega,0)\|}$ comparable with **MONS** were calculated for stilbazolium derivative **17** (Table 4). The results also show that the dinitrogen derivatives **8** are half as efficient chromophores as the pyridinium derivatives **2b** and **3b**.

NLO properties of the cluster derivatives were also compared with those for pyridine and stilbazole complexes with BH_3, **18** and **19**, respectively, in which borane acts only as Lewis acid. Data in Table 4 show that the complexes are significantly less efficient than {*closo*-B_{10}} derivatives and standard organic NLO chromophores. These results are in agreement with our original calculations at the AM1 level of theory[22] and later experimental[44] and computational studies[45] of BF_3 and $B(C_6F_5)_3$ complexes.

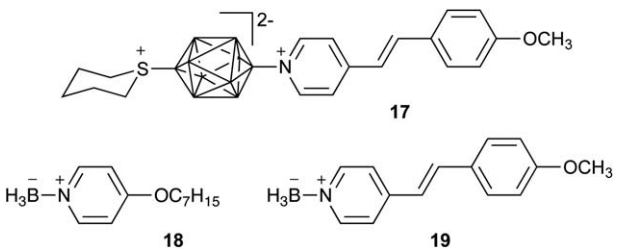

Measurements for **2b** by the hyper-Rayleigh scattering method[41,46] in CH_2Cl_2 solutions gave the value of $\beta^{HRS} = 45 \pm 10 \times 10^{-30}$ esu at 1064 nm, which is comparable to computational results (Table 4) and nearly twice larger than experimental values $\beta_{z(2\omega)}$ obtained for **PNA**[41] and **DMANB**[43] using the EFISHG method.[47]

Our previous investigation of a thin film of **2b** sandwiched between ITO glass showed that a reversible weak SHG signal

Table 4 Calculated first hyperpolarizability and molecular dipole for selected compounds in CH_2Cl_2[a]

	$\beta_{(-\omega,\omega,0)\|}$ (esu)		$\beta_{(1064)}$ (esu)		
Compound	$\omega = 0$	$\omega = 1064$ nm	Exp.	μ_g (D)	$\mu_\|$ (D)
2b[c]	17.5	20.0	45 ± 10[d,e]	4.85	4.11
3b	28.0	31.2	—	3.40	3.17
8a[c]	12.2	10.0	—	8.92	8.88
8b	14.2	11.9	—	9.64	9.57
17	293.1	164.0	—	7.45	7.26
18	0.75	0.59	—	10.22	9.03
19	79.6	81.3	—	12.59	12.59
PNA	20.0	17.9	23 ± 3[d,f] 34.5[g,h]	8.98	8.93
DMANB	26.1	23.5	26 ± 8[g,i]	9.71	9.66
MONS	203.7	231.5	105 ± 35[d,j]	9.59	9.56

[a] Obtained with the B3LYP/6-31G(d,p)||B3LYP/6-31G(d,p) method in CH_2Cl_2 dielectric medium. [b] β is the vector part of hyperpolarizability tensor projected along the dipolar axis of the molecule. [c] For *trans* isomer only. [d] HRS method. [e] This work. [f] In $CHCl_3$, ref. 41; calcd $\beta_{(-\omega,\omega,0)\|_i} = 16.8 \times 10^{-30}$ esu in $CHCl_3$. [g] EFISHG method. [h] In $CHCl_3$, ref. 42. [i] Ref. 43. [j] In $CHCl_3$, ref. 41; calcd value $\beta_{(-\omega,\omega,0)\|} = 174.5 \times 10^{-30}$ esu in $CHCl_3$.

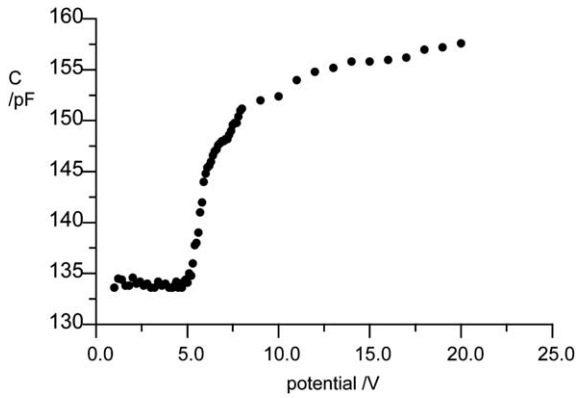

Fig. 13 Capacitance *C vs.* applied voltage measured for an electrooptical cell containing **2b** at 130 °C.

was generated upon glassification of the nematic phase below 90 °C.[24] Analysis of the efficiency of the main component of the second-order nonlinear susceptibility $\chi_{zzz} = 2.3 \pm 0.3$ pm V^{-1} along the nematic director z, demonstrated that it corresponded to about 0.3% of molecules exhibiting spontaneous polar order. The origin of this effect remains unclear.

Dielectric measurements

Dielectric parameters for **2b** were obtained in a planar cell at 130 °C by the single cell method.[48] Analysis of capacitance as a function of applied voltage (Fig. 13) gave dielectric parameters $\varepsilon_{\|} = 6.1 \pm 0.1$, $\varepsilon_{\perp} = 4.8 \pm 0.1$ and $\Delta\varepsilon = +1.3 \pm 0.1$. The positive dielectric anisotropy of the material is consistent with a calculated moderate molecular dipole moment of 4.33 D oriented at $\beta = 30°$ relative to the long molecular axis in the *trans* isomer, while in the *cis* isomer the net dipole moment is larger (6.25 D) and the β is 44° in a vacuum. The dielectric results were analyzed using the Maier–Meier relationship connecting molecular and bulk parameters of the material.[49,50] Assuming that at 130 °C the ratio of **2b-*trans*** to **2b-*cis*** (two principal species, Fig. 7) is 2.76 (extrapolated from the equilibrium data, *vide supra*), the average molecule can be represented by 73.4% of **2b-*trans*** and 26.6% **2b-*cis***. Maier–Meier analysis[3,5] for such a molecule gives an order parameter S of only 0.25, and the Kirkwood factor $g = 0.48$. The same analysis for a more typical value of $S = 0.6$ and $g = 0.5$ for the pure **2b-*trans*** isomer gave $\varepsilon_{\|} = 7.0$ and $\Delta\varepsilon = +3.2$.

Discussion

The chemistry of the {*closo*-B_{10}} cluster permits the preparation of unsymmetric derivatives **2** and **3** by sequential introduction of the onium fragments Q^+. The overall yield of the 5 step synthesis is only about 5% based on [*closo*-$B_{10}H_{10}]^{2-}$ (**I**), with the last step, substitution of the pyridinium fragment for N_2 in **8**, being particularly inefficient. The mechanism for this transformation involves thermally induced heterolysis of the B–N bond and formation of boronium ylide **20**, which is trapped with a Lewis base L (Scheme 6). DFT calculations for model compound **16** demonstrate that the energetics of this S_N1 substitution reaction are similar to those found for analogous derivatives of the {*closo*-1-CB_9} cluster.[27] Thus, the formation of the ylide **20c** from **8c** (Q = thian) is moderately endothermic by $\Delta H = 37.9$ kcal mol^{-1}, while trapping of **20c** with 4-methoxypyridine and formation of **16** is significantly exothermic ($\Delta H = -67.4$ kcal mol^{-1}). Ylide **20** is a reactive intermediate, and besides reacting with the Lewis basic center (N in pyridines), also inserts to the C–H bonds.[17] Thus, for larger molecules, the yield of the desired product diminishes due to higher ratio of C–H bonds to the Lewis center.

Bis-onium derivatives exhibit some hydrolytic and thermal instability. For instance, pyridine derivatives **2**, and to a lesser extent **1** and **3**, appear to be sensitive to light and moisture. This is presumably related to an increased susceptibility of the {*closo*-B_{10}} cluster to attack and cage opening by nucleophiles, such as water, upon photoexcitation. Support for this is provided by ^{1}H NMR spectroscopy, which shows loss of symmetry by the cage and upfield shift of the pyridine H atoms in solid **2b** that was exposed to ambient conditions for several weeks.

The {*closo*-B_{10}} cluster substituted with onium fragments is configurationally unstable above 200 °C and 1,10-disubstituted derivatives rearrange to other isomers.[20,51] For instance [*closo*-$B_{10}H_8$-1,10-$(SMe_2)_2$] gave nearly 3% of the [*closo*-$B_{10}H_8$-2,7(8)-$(SMe_2)_2$] isomer after 45 min at 230 °C.[20] This is consistent with the observed partial decomposition and possible rearrangement of *e.g.* **3b** upon melting at 285 °C.

Despite limited stabilities, quinuclidinium, thianium, and 4-alkoxypyridinium substituents investigated in this work appear to be most suitable for the formation of liquid crystalline derivatives of the [*closo*-$B_{10}H_{10}]^{2-}$ cluster. Other types of onium fragments, are less suitable for structure **II** due to their low thermal stability (–N_2) or hydrolytic instability (–CO, –NCR).[17]

The effectiveness of the ring in promoting crystalline phase in **1–5** appears to follow the order: thian < pyridine < quinuclidine. The pyridine ring is also more effective than thian in stabilizing the nematic phase. However, on the basis of the ring size and fill fraction, pyridine is expected to be the least effective in phase stabilization. The lowest effectiveness of the thian is presumably related to its facile epimerization at the *S* center similar to that reported for **21**,[4] a B(10)-sulfonium derivative of the [*closo*-1-$CB_9H_{10}]^-$ cluster, and equilibrium with the *cis* isomer. The relatively low activation energy of the isomerization in **2b** ($\Delta H^{\ddagger} = 23.5 \pm 0.6$ kcal mol^{-1}) is nearly identical to that measured for sulfonium ylide **22**,[52,53] and involves pyramidal inversion[54] with the participation of the adjacent π-symmetry electron manifold of the {*closo*-B_{10}} cluster. For comparison, the barrier to epimerization in sulfoxide **23** is significantly higher.[55]

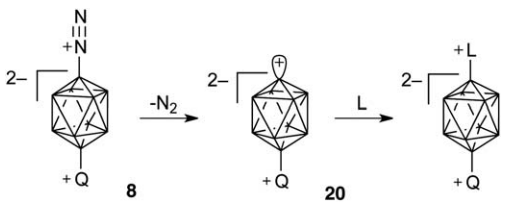

Scheme 6

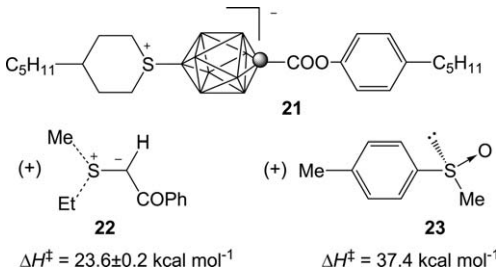

The rather small value of the steric factor A (0.82 kcal mol^{-1}) for the {*closo*-B_{10}} cluster in thian derivatives such as **2** and **8a** results in a significant population of the *cis* isomer in equilibrium, which destabilizes the nematic phase and inhibits crystallization. However, a comparison with other groups substituted at the sulfur atom in the thian demonstrates that the {*closo*-B_{10}} cluster is relatively big, and its factor A is nearly 3 times larger than that for the Me group[56,57] (Table 5). The generally low values of steric factors A in thian derivatives, when compared to cyclohexane analogues (Table 5), are due to relatively long bonds to the sulfur atom (about 1.85 Å *vs.* 1.54 Å) and consequently lesser contact between the substituent and the 1,3-axial hydrogen atoms. For instance, the B–S bond in **2b-*trans*** is d_{B-S} = 1.850 Å *avg* (Fig. 4). For comparison, the B(10)–S bond in a similar derivative of the isoelectronic and nearly isosteric {*closo*-1-CB_9} cluster ([*closo*-1-CB_9H_8-10-SC_5H_{10}-1-COOH])[27] is slightly longer (d_{B-S} = 1.858 Å, and consequently the A factor of the boron cage in ester **21** is lower by 0.05 kcal mol^{-1}.[4] The difference in the B–S bond distance in the two mesogens is also reproduced computationally for the *cis* isomers in which the boron cluster is in the axial position: d_{B-S} = 1.879 Å for **2b-*cis*** and d_{B-S} = 1.886 Å for **21-*cis***. In derivatives of {*closo*-1-CB_9} in which the cluster is connected to the thian through the carbon atom, the C(1)–S distance is shorter[4] than in **2b**, and *cis* isomers are not observed experimentally.[5]

Thus, thian derivatives **2** exist as a mixture of interconverting *cis* and *trans* isomers, which impacts the stability of the nematic phase and ability to crystalize. This situation is even more complicated for bis-sulfonium **4**, which exists as a mixture of 3 isomers, and consequently does not exhibit liquid crystalline properties. The two isomers in **2** interconvert slowly at ambient temperature (half-life of the *trans* isomer is τ = 13 min), while above 100 °C the interconversion between linear and bent forms of the same molecule is fast (τ = 20 ms at 130 °C, extrapolated from solution data). The existence of the mixture causes supercooling and glassification of the nematic phase of **2b**, however, during crystallization configurational selection takes place and only the *trans* isomer forms the crystalline phase, according to NMR analysis.

The effect of the alkoxy group structure on phase transition temperatures in **2** is surprisingly large. For instance, branching of an alkyl chain causes phase destabilization, which can be estimated by comparison of pairs of structurally similar compounds. According to a correlation of T_{NI} for mesogens containing 4-C_7H_{15}OPh – with those with the 4-C_6H_{13}CHMeOPh– fragment (T_{NI} = 0.78 × T_2 + 105; r = 0.97, n = 13),[1] the expected N–I transition for **2e** is 71 °C, and the melting point around 110 °C. However, the observed temperatures are lower than predicted by more than 50 K! Such a significant difference suggests that intermolecular polar interactions are important for phase stability, which are weakened by α-branching of the alkoxy chain and shielding access to the pyridine ring. These interactions are evident from the single crystal structure of **2b** in which the distance between the B–N bonds of neighboring molecules is 6.3 Å and the closest B···C intermolecular distance is 3.75 Å (Fig. 14). This analysis implies that the appearance of a broad-range nematic phase in **2b** and also in **2c** results, in part, from strong intermolecular polar interactions.

In series **3** this effect of polar interactions appears to be less important, and the difference of 19 K in the melting point between **3b**, containing the heptyloxy chain, and **3e** with the 1-methylheptyloxy substituent is within expectations. Instead, efficient space filling with rigid cylindrical quinuclidine and the

Table 5 Steric parameter $A = -\Delta G^{o}_{298}$ for selected substituents in cyclohexane and thiane

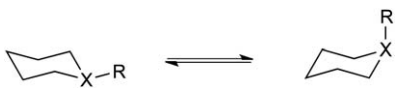

	$-\Delta G^{o}_{298}$/kcal mol^{-1}	
R	X = CH	X = S$^+$
O$^-$	(1.04)[a]	−0.175[b]
NH$^-$	(1.47)[c]	0.075[d]
Me	1.74[e]	0.275[f]
PhCON	(1.6)[g]	−0.16[h]
21	—	0.77[i]
2b	—	0.82[j]

[a] Value for OH in CS_2, ref. 58. [b] At 183 K, ref. 59. [c] Value for NH_2 in toluene-d_8, ref. 60. [d] At 188 K, CH_2Cl_2/$CHClF_2$, ref. 61. [e] Ref. 62. [f] At 373 K in $CDCl_3$, ref. 56 and 57. [g] Value for PhCONH, ref. 63. [h] At 201 K in CH_2Cl_2/acetone-d_6, ref. 64. [i] Ref. 4. [j] This work.

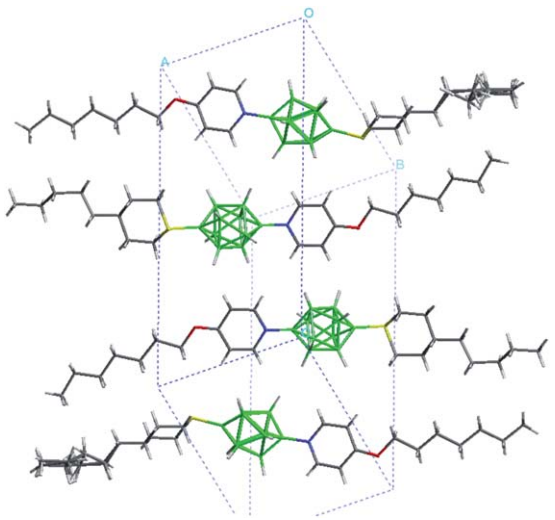

Fig. 14 Molecular packing in the unit cell of **2b**.

{*closo*-B_{10}} cluster becomes the dominant factor stabilizing the crystalline phase. The stability of the crystalline phase increases further upon substitution of the pyridinium ring with the second quinuclidinium substituent in **5**.

Branching at the β-carbon atom of the alkoxy chain typically lowers the melting point, as is evident from a comparison of a number of pairs with isomeric pentyloxy and 2-methylbutoxy substituents.[1] Instead, experiments show that the β-branched derivative **2d** has higher stability of the solid phase by 25 K than **2a**, which is 40 K higher than expected. A correlation of T_{NI} for pairs containing either 4-$C_5H_{11}OPh$– or 4-$C_2H_5CHMeCH_2OPh$– fragment ($T_{NI} = 0.90 \times T_2 + 44$; $r = 0.99$, $n = 69$) predicts the N–I transition for **2d** at 131 °C, which is significantly below melting.

Bis-betains of structure **II** have high longitudinal quadrupole moment q arising from two opposing each other strong local dipoles associated with the cluster–onium bonds. For instance, in **1a** the longitudinal component of the quadrupole moment $q_{xx} = 118.3$ D Å and in **2b-*trans*** $q_{xx} = 86.5$ D Å. The local dipole moments only partially cancel out, and even in symmetric derivatives there is a residual net ground state dipole moment related to the D_{4d} symmetry of the boron cluster. For instance, in **1a** with the D_2 point group symmetry, the transverse dipole moment component is $\mu_\perp = 1.20$ D. In dissymmetric derivatives **II** the net ground state dipole moment depends on the substituents and varies from 3.40 D for **3b** to 9.64 D for **8b** and is oriented along the long molecular axis. Consequently such compounds have $\Delta\varepsilon > 0$ and undergo electrooptical switching, as was demonstrated for **2b**.

Computational and experimental results for selected derivatives of the $[closo\text{-}B_{10}H_{10}]^{2-}$ cluster (**I**) in Table 4 demonstrated that compounds **2** and **3** are moderately efficient NLO chromophores. Their molecular hyperpolarizability β values are similar to those of carborane and ionic $[closo\text{-}B_{12}H_{12}]^{2-}$ derivatives[8] and comparable with simple organic NLO chromophores with the classical architecture *Donor*–π Linker–*Acceptor*. However, derivatives **2** and **3** appear to be more efficient NLO chromophores than their closest structural analogues, ylide [*closo*-1-$CB_{11}H_{11}$-12-C_7H_6] ($\beta^{HRS} = 7.2 \times 10^{-30}$ esu),[65] and *N*-phenoxide-pyridinium betaines ($\beta_{xxx} = 8.8$–34×10^{-30} esu).[66] Much higher β values are predicted for systems in which the boron cluster is a bridge between a strong donor and acceptors, such as tropylium and cyclopentadienyl, and the cluster acts as a conduit of electron transfer in the excitation process.[67]

In chromophores derived from **I**, the boron cluster serves a dual role: the electron donor and a Lewis acid directly bonded to the acceptor, the pyridinium ring (*Donor–Acceptor*). In compounds derived from mono-boranes, such as BR_3,[44] the borane serves only as a Lewis acid and, consequently, the molecular hyperpolarizability β is lower than for cluster derivatives such as **2** and **3**. In spite of the moderate β values, it appears that derivatives of $[closo\text{-}B_{10}H_{10}]^{2-}$, such as **2** and **3**, may have advantage over conventional molecular NLO systems by having low ground state dipole moment and being transparent above 400 nm, providing that non-centrosymmetric bulk structure could be obtained.

Conclusions

We have demonstrated that substitution of the $[closo\text{-}B_{10}H_{10}]^{2-}$ cluster at the apical positions with appropriate onium groups Q^+ leads to bis-betains **II** in which polar and photophysical properties (solvatochromism, absorption/emission energy, hyperpolarizability) can be adjusted and liquid crystalline behavior can be induced. Besides bis-pyridinium **1**, only *n*-alkoxypyridinium derivatives **2** exhibit mesophase and they form a nematic phase above 100 °C. Results of structure–property relationship studies aided by the LiqCrys database suggest that polar intermolecular interactions play an important role in the stability of both crystalline and nematic phases.

Molecules of compounds containing the thian ring (**2**) are conformationally and configurationally labile, and they exists as a mixture of interconverting isomers in a fluid phase. It is estimated that up to 30% of the *cis* isomer co-exists with the *trans* form in the liquid crystal phase (120–160 °C), which affects the crystallization process and results in glass formation. Interestingly, crystallization proceeds with configurational selection for the *trans* isomer.

Electronic structure of the 10-vertex *closo*-boranes permits efficient electronic communication with π-substituents such as pyridinium in **1–3** and dinitrogen in **8**. In heterodisubstituted derivatives, in which one onium group has a π and another σ character, directional photoexcitation eliminates one of the local dipole moments and increases the net molecular dipole moment. Such compounds exhibit a negative solvatochromic effect and have a moderate value for the first hyperpolarizability β, similar to those of conventional organic NLO materials of comparable size.

Computational details

Quantum-mechanical calculations were carried out with the B3LYP[68,69] method with 6-31G(d,p) basis set using Gaussian 09 package.[70] Details of ground and transition state geometry optimization, electronic excitation energies and hyperpolarizability calculations, and solvation effects are provided in the ESI.‡

Experimental part

General

NMR spectra were obtained at 300 or 400 MHz (^{1}H), 75 MHz (^{13}C), and 128 MHz (^{11}B) respectively, in CD_3CN or $CDCl_3$. Chemical shifts were referenced to the solvent (^{1}H, ^{13}C) or to $B(OMe)_3$ (external sample). IR spectra were recorded by deposition of a thin film from solution onto sodium chloride disks. Dry DMSO was prepared by using molecular sieves that were activated in a microwave oven. Thermal analysis was performed on TA 2920 DSC using a typical heating rate of 5 K min^{-1}. Fluorescence quantum yield was established according the literature protocol using quinine bisulfate solution in 0.1 N H_2SO_4 as a reference.[38] Details are described in the ESI.‡

Trans–cis equilibrium measurements

A solution of **2b** in toluene-d_8 was equilibrated at a constant temperature for 2 h before each measurement in the range of 50–100 °C every 10 K. The mole fraction α of the *cis* isomer was obtained at each temperature by integration of low field ^{1}H NMR signals as described below. Thermodynamic parameters were calculated by plotting $\ln(\alpha)$ *vs.* $1/T$. For details see ESI.‡

Isomerization of 2b-*trans*. Kinetic measurements

A crystalline sample of **2b** (~10 mg) was dissolved in toluene-d_8 (0.6 mL) in an NMR tube at ice bath temperature and inserted into a precooled NMR instrument (400 MHz). Spectra were referenced to the Ph-CD_2H quintet at 2.09 ppm. The sample was kept at a constant temperature (0–25 °C) and ^{1}H NMR spectra were taken at regular time intervals until little change was observed (>3× half-life). The low field portion of the NMR spectrum was processed in MestReC program version 4.3.6.0: (http://www.MestReC.com) the partially overlapping pseudo-doublets of the AA′XX′ patterns for both isomers were deconvoluted and areas were calculated using the Line Fitting tool. The areas of the downfield wing of the major pseudo-doublet and the upfield wing of the minor pseudo-doublet were used for calculation of the mole fraction α of the *cis* isomer **2b-*cis***.

Data analysis. The mole fraction of the *cis* isomer at the infinite time (α_∞) was calculated at each temperature T from the extrapolated equilibrium constant K_T (*vide supra*). Rate constants were obtained from plots of $\ln(\alpha_\infty - \alpha)$ against $1/T$ and are listed in the ESI.‡

Dielectric measurements

Dielectric parameters were obtained from Liquid Crystal Analytical System – Series 1 (LCAS). A sample of **2b** was placed into a 9.1 μm thick cell (optical measurements) with a rubbed SiO_2 layer. Ten scans were taken for each of three different cells at a 1 kHz triangular shape voltage applied with an amplitude between 0.1 V and 20 V, and the results were averaged. Each empty cell was measured by LCAS ("cell nulling") before filling with **2b** by capillary forces at about 140 °C. Subsequently, the filled cells were heated to the isotropic phase for a short time, and quickly cooled to 130 °C for dielectric measurements.

General procedure for the preparation of pyridine derivatives 2 and 3

A solution of dinitrogen derivative **8** (1.0 mmol) in appropriate 4-alkoxypyridine **10** (5 mL) was stirred at 120 °C overnight. Excess pyridine was distilled off under reduced pressure and the semicrystalline residue was passed through a silica gel plug (hexane–CH_2Cl_2, 1 : 2) giving crude product in about 30% yield. Further purification was accomplished by column chromatography (hexane–CH_2Cl_2) followed by repeated recrystallization.

1-(4-Pentyloxypyridinyl)-10-(4-pentyl-1-thiacyclohexyl)-*closo*-decaborane (2a)

The product was recrystallized (3×, iso-octane–toluene, 1 : 1) yielding a white crystalline solid: ^{1}H NMR (400 MHz, $CDCl_3$) major signals δ 0.5–2.0 (br m, 8H), 0.91 (t, J = 7.0 Hz, 3H), 0.97 (t, J = 8.0 Hz, 3H), 1.25–1.35 (m, 8H), 1.36–1.53 (m, 6H), 1.56–1.75 (m, 3H), 1.91 (quint, J = 7.0 Hz, 2H), 2.32 (br d, J = 13.8 Hz, 2H), 3.44 (t, J = 13.1 Hz, 2H), 3.68 (br d, J = 13.0 Hz, 2H), 4.23 (t, J = 6.5 Hz, 2H), 7.13 (d, J = 7.3 Hz, 2H), 9.29 (d, J = 7.3 Hz, 2H); ^{11}B NMR (128 MHz, $CDCl_3$) δ −25.8 (4B), −25.0 (4B), 4.2 (1B), 21.3 (1B).

Distinct signals ascribed to the **2a-*cis*** isomer (23% int): ^{1}H NMR (400 MHz, $CDCl_3$) δ 1.98–2.07 (m), 2.41–2.52 (m), 3.34 (ddd, J_1 = 13.6 Hz, J_2 = 10.5 Hz, J_3 = 3.3 Hz), 3.52–3.58 (m).

Anal. calcd for $C_{20}H_{43}B_{10}NOS$: C, 52.94; H, 9.55; N, 3.09. Found: C, 53.20; H, 9.38; N, 3.07%.

1-(4-Heptyloxypyridinyl)-10-(4-pentyl-1-thiacyclohexyl)-*closo*-decaborane (2b)

Yellowish crude solid product was purified by chromatography (SiO_2, hexanes–CH_2Cl_2, 2 : 1) and recrystallized from EtOH followed by an iso-octane–toluene mixture giving white crystals: ^{1}H NMR (400 MHz, $CDCl_3$) major signals δ 0.5–2.0 (m, 8H), 0.91 (t, J = 6.9 Hz, 3H), 0.92 (t, J = 6.8 Hz, 3H), 1.26–1.42 (m, 14H), 1.47–1.54 (m, 2H), 1.56–1.75 (m, 3H), 1.91 (quint, J = 7.0 Hz, 2H), 2.32 (br d, J = 13.8 Hz, 2H), 3.44 (t, J = 12.9 Hz, 2H), 3.69 (br d, J = 12.8 Hz, 2H), 4.23 (t, J = 6.5 Hz, 2H), 7.13 (d, J = 7.4 Hz, 2H), 9.30 (d, J = 7.3 Hz, 2H); ^{13}C NMR (75 MHz, DEPT-135, $CDCl_3$) major signals δ 14.0 (CH_3), 22.5, 25.6, 26.0, 28.5, 28.8, 31.2, 31.6, 31.8, 36.1 (CH), 36.4, 41.8, 70.1, 111.7 (CH), 149.1 (CH), 168.7 (C); ^{11}B NMR (128 MHz, CD_3CN) major signals δ −26.1 (4B), −25.4 (4B), 3.7 (1B), 20.8 (1B).

Distinct signals ascribed to the **2b-*cis*** isomer: ^{1}H NMR δ 3.52–3.59 (m), 3.34 (ddd), 2.41-2.52 (m), 1.98–2.06 (m); ^{13}C NMR δ 26.1, 26.6, 33.9, 34.6, 36.0; ^{11}B NMR δ 1.4.

UV (MeCN) λ_{max} (log ε) 301 nm (4.12), 232 (4.19); HRMS, calcd for $C_{22}H_{47}B_{10}NOS$: m/z 483.4309; found: m/z 483.4337. Anal. calcd for $C_{22}H_{47}B_{10}NOS$: C, 54.85; H, 9.83; N, 2.91, S, 6.65. Found: C, 55.08; H, 9.89; N, 2.98, S, 6.59%.

1-(4-Nonyloxypyridinyl)-10-(4-pentyl-1-thiacyclohexyl)-*closo*-decaborane (2c)

^{1}H NMR (400 MHz, $CDCl_3$) major signals δ 0.5–2.0 (m, 8H), 0.90 (t, J = 7.0 Hz, 3H), 0.91 (t, J = 6.8 Hz, 3H), 1.26–1.42 (m, 18H), 1.47–1.54 (m, 2H), 1.56–1.75 (m, 3H), 1.91 (quint, J = 7.0 Hz, 2H), 2.31 (br d, J = 11.9 Hz, 2H), 3.44 (t, J = 13.3 Hz, 2H), 3.68 (br d, J = 13.3 Hz, 2H), 4.23 (t, J = 6.5 Hz, 2H), 7.13 (d, J = 7.4 Hz, 2H), 9.30 (d, J = 7.3 Hz, 2H).

Distinct signals ascribed to the **2c-*cis*** isomer: ^{1}H NMR δ 3.52–3.59 (m), 3.34 (ddd), 2.41–2.52 (m), 1.98–2.06 (m).

Anal. calcd for $C_{24}H_{51}B_{10}NOS$: C, 56.54; H, 10.08; N, 2.75. Found: C, 56.81; H, 10.18; N, 2.75%.

1-(4-[(*S*)-2-Methyl-1-butoxypyridinyl])-10-(4-pentyl-1-thiacyclohexyl)-*closo*-decaborane (2d)

Column chromatography (SiO_2, CH_2Cl_2–hexane, 1 : 2) gave **2d** as white crystals (34% yield), which were recrystallized from an iso-octane–toluene mixture: ^{1}H NMR (400 MHz, $CDCl_3$) major signals δ 0.5–2.0 (m, 8H), 0.91 (t, J = 7.0 Hz, 3H), 1.00 (t, J = 7.5 Hz, 3H), 1.09 (d, J = 6.7 Hz, 3H), 1.25–1.38 (m, 10H),

1.55–1.73 (m, 4H), 1.94–2.07 (m, 1H), 2.30 (d, $J = 13.5$ Hz, 2H), 3.44 (t, $J = 13.0$ Hz, 2H), 3.68 (d, $J = 13.0$ Hz, 2H), 4.01 (dd, $J_1 = 9.1$ Hz, $J_2 = 6.6$ Hz, 1H), 4.09 (dd, $J_1 = 9.1$ Hz, $J_2 = 6.0$ Hz, 1H), 7.14 (d, $J = 7.4$ Hz, 2H), 9.30 (d, $J = 7.3$ Hz, 2H).

Distinct signals ascribed to the **2d-*cis*** isomer: ^{1}H NMR δ 3.52–3.59 (m), 3.34 (ddd), 2.42–2.52 (m).

Anal. calcd for $C_{20}H_{43}B_{10}NOS$: C, 52.94; H, 9.55; N, 3.09. Found: C, 53.18; H, 9.62; N, 3.07%.

1-(4-[(*S*)-2-Octyloxypyridinyl)])-10-(4-pentyl-1-thiacyclohexyl)-*closo*-decaborane (2e)

Chromatography (SiO_2, CH_2Cl_2–hexane, 1 : 2) gave **2d** as a viscous oil: ^{1}H NMR (400 MHz, $CDCl_3$) major signals δ 0.5–2.0 (m, 8H), 0.90 (t, $J = 7.1$ Hz, 3H), 0.91 (t, $J = 7.0$ Hz, 3H), 1.22–1.38 (m, 14H), 1.44 (d, $J = 6.1$ Hz, 3H), 1.56–1.76 (m, 6H), 1.80–1.91 (m, 1H), 2.30 (br d, $J = 13.6$ Hz, 2H), 3.44 (br t, $J = 13.0$ Hz, 2H), 3.67 (br d, $J = 12.9$ Hz, 2H), 4.67 (sext, $J = 6.2$ Hz, 1H), 7.09 (d, $J = 7.4$ Hz, 2H), 9.27 (d, $J = 7.3$ Hz, 2H).

Distinct signals ascribed to **2e-*cis*** isomer: ^{1}H NMR δ 3.52–3.59 (m), 3.33 (ddd), 2.42–2.52 (m), 1.99–2.07 (m).

HRMS, calcd for $C_{23}H_{49}B_{10}NOS$: *m/z* 496.4501; found: *m/z* 496.4508.

1-(4-Heptyloxypyridinyl)-10-(4-pentyl-1-quinuclidinyl)-*closo*-decaborane (3b)

Crude yellowish product was recrystallized from MeCN and then from a toluene–iso-octane mixture (2×) to give white crystals: ^{1}H NMR (400 MHz, $CDCl_3$) δ 0.5−2.0 (m, 8H), 0.91 (t, $J = 7.1$ Hz, 3H), 0.92 (t, $J = 7.0$ Hz, 3H), 1.25–1.42 (m, 16H), 1.45–1.52 (m, 2H), 1.85 (t, $J = 7.8$ Hz, 6H), 1.85–1.92 (m, 2H), 4.06 (t, $J = 8.0$ Hz, 6H), 4.21 (t, $J = 6.5$ Hz, 2H), 7.10 (d, $J = 7.4$ Hz, 2H), 9.31 (d, $J = 7.4$ Hz, 2H); ^{1}H NMR (300 MHz, benzene-d_6) δ 0.5–2.0 (m, 8H), 0.85–1.05 (m, 14H), 1.10–1.45 (m, 14H), 3.11 (t, $J = 6.3$ Hz, 2H), 3.78 (t, $J = 7.9$ Hz, 6H), 5.91 (d, $J = 7.2$ Hz, 2H), 9.07 (d, $J = 7.2$ Hz, 2H); ^{13}C NMR (75 MHz, benzene-d_6) δ 14.3, 23.0, 23.2, 25.9, 27.4, 28.6, 29.2, 29.8, 32.0, 32.7, 40.4, 58.6, 69.2, 111.0, 149.3, 167.7; ^{11}B NMR (128 MHz, $CDCl_3$) δ −29.4 (4B), −28.1 (4B), 15.6 (1B), 17.9 (1B); UV (MeCN), λ_{max} (log ε) 310 nm (4.05), 233 nm (4.11); HRMS calcd for $C_{24}H_{50}B_{10}N_2$ *m/z* 492.4854; found: *m/z* 492.4879. Anal. calcd for $C_{24}H_{50}B_{10}N_2O$: C, 58.73; H, 10.27; N, 5.71. Found: C, 58.91; H, 10.19; N, 5.69%.

1-(4-[(*S*)-2-Octyloxypyridinyl)])-10-(4-pentyl-1-quinuclidinyl)-*closo*-decaborane (3e)

Pure product was obtained by crystallization from an iso-octane–toluene mixture and then toluene: ^{1}H NMR (400 MHz, $CDCl_3$) δ 0.5–2.5 (brm, 8H), 0.91 (t, $J = 7.0$ Hz, 3H), 0.93 (t, $J = 6.8$ Hz, 3H), 1.26–1.42 (m, 18H), 1.44 (d, $J = 6.1$ Hz, 3H), 1.68–1.76 (m, 2H), 1.85 (t, $J = 7.9$ Hz, 8H), 4.06 (t, $J = 8.0$ Hz, 6H), 4.65 (sext, $J = 6.0$ Hz, 1H), 7.07 (d, $J = 7.4$ Hz, 2H), 9.30 (d, $J = 7.4$ Hz, 2H). Anal. calcd for $C_{25}H_{52}B_{10}N_2O$: C, 59.48; H, 10.38; N, 5.55. Found: C, 59.42; H, 10.26; N, 5.45%.

1,10-Bis(4-pentyl-1-thiacyclohexyl)-*closo*-decaborane (4)

A solution of bisdinitrogen [*closo*-$B_{10}H_8$-1,10-$(N_2)_2$] (**12**, 86 mg, 0.50 mmol) in 4-pentylthian[71] (**14**, 2 mL) was stirred at 120 °C for 18 h. Excess thian was removed under reduced pressure, and the residue was passed through a silica gel plug (CH_2Cl_2). Pure product **4** was isolated by column chromatography (first hexane, then CH_2Cl_2–hexane, 1 : 1, 42 mg, 18% yield) followed by repeated recrystallization (hexane/EtOAc): ^{1}H NMR (400 MHz, $CDCl_3$) major signals δ 0.5–2.5 (brm, 8H), 0.91 (t, $J = 7.0$ Hz, 6H), 1.25–1.40 (m, 18H), 1.60–1.75 (m, 4H), 2.32 (br d, $J = 13.8$ Hz, 4H), 3.44 (t, $J = 12.8$ Hz, 4H), 3.69 (br d $J = 12.5$ Hz, 4H); ^{11}B NMR (128 MHz, $CDCl_3$) δ −24.4 (8B) 10.1 (2B).

Distinct signals ascribed to **4-*cis*** isomer present in about 25%: ^{1}H NMR δ 0.85–0.89 (t), 2.00–2.09 (m), 2.39–2.50 (m) 3.28–3.39 (m), 3.52–3.60 (m).

Anal. calcd for $C_{20}H_{48}B_{10}S_2$: C, 52.13; H, 10.50. Found: C, 52.20; H, 10.41%.

1,10-Bis(4-pentyl-1-quinuclidinyl)-*closo*-decaborane (5)

A mixture of crude diamine [*closo*-$B_{10}H_8$-1,10-$(NH_3)_2$] (**13**, 57 mg, 0.37 mmol),[37] 3,3-bis(2-bromoethyl)-1-bromooctane[28] (**11**, 305 mg, 0.75 mmol), dicyclohexyl-18-crown-6 (7 mg, 0.03 mmol), anhydrous K_2CO_3 (280 mg, 2.0 mmol) and dry MeCN (5 mL) was stirred under reflux for 5 days under Ar. The suspension was filtered and the solid was washed with MeCN. The crude product was purified on a silica gel plug (CH_2Cl_2–hexane, 1 : 1) to give 34 mg (28% yield) of **5** as white crystals, which was recrystallized from iso-octane–toluene and then toluene: ^{1}H NMR (400 MHz, $CDCl_3$) δ 0.5–2.3 (brm, 8H), 0.91 (t, $J = 6.9$ Hz, 6H), 1.26–1.38 (m, 16H), 1.83 (t, $J = 7.9$ Hz, 12H), 4.02 (t, $J = 7.9$ Hz, 12H); ^{13}C NMR (75 MHz, $CDCl_3$) δ 14.0, 22.6, 23.1, 27.9, 29.6, 30.3 (3C), 32.4, 40.3, 58.6 (3C); ^{11}B NMR (128 MHz, $CDCl_3$) δ −29.1 (d, $J = 124$ Hz, 8B), 18.2 (s, 2B). Anal. calcd for $C_{24}H_{54}B_{10}N_2$: C, 60.20; H, 11.37; N, 5.85. Found: C, 60.18; H, 11.21; N, 5.73%.

1-(4-Pentyl-1-thiacyclohexyl)-*closo*-decaborate $[NMe_4]^+$ (7c[NMe_4])

A mixture of crude [*closo*-$B_{10}H_9$-1-$SCHNMe_2$]$^-$[NMe_4]$^+$ (**7a [NMe_4]**, 9.00 g, 31.4 mmol),[37] 1,5-dibromo-3-pentylpentane[26] (**9**, 9.3 g, 31.4 mmol), $NMe_4OH\cdot5H_2O$ (14 g, 85 mmol), and MeCN (100 mL) was stirred for 24 h at room temperature. The mixture was filtered to remove inorganic solids and the filtrate was evaporated. The residue was treated with CH_2Cl_2 and the mixture was filtered through a silica gel plug, which was washed well with MeCN–CH_2Cl_2 (2 : 1). The eluate was evaporated, the residue extracted into warm hexane–CH_2Cl_2 (1 : 10), and the extract was evaporated to give 6.20 g (53% yield) of a pale yellow solid material: ^{1}H NMR (400 MHz, CD_3CN) major signals δ −0.6 to 1.4 (br m, 8H), 0.91 (t, $J = 6.8$ Hz, 3H), 1.26–1.40 (m, 6H), 1.60–1.68 (m, 3H), 2.25–2.32 (m, 2H), 3.07 (s, 12H), 3.25–3.40 (m, 4H), 3.60 (br d, $J = 12.5$ Hz, 2H), 3.9 (br q, $J = 154$ Hz, 1H); ^{11}B NMR (128 MHz, CD_3CN) δ −27.7 (d, $J = 131$ Hz, 4B), −25.3 (d, $J = 125$ Hz, 4B), 0.1 (s, 1B), 8.4 (d, $J = 154$ Hz, 1B).

Distinct signals ascribed to **7c[NMe_4]-*cis*** isomer present in about 25%: ^{1}H NMR δ 0.85–0.89 (m), 2.41–2.50 (m); ^{11}B NMR δ −1.9 (s).

Anal. calcd for $C_{14}H_{41}B_{10}NS$: C, 46.24; H, 11.36; N, 3.85. Found: C, 46.46; H, 10.85; N, 3.77%.

1-(4-Pentyl-1-quinuclidinyl)-*closo*-decaborate $[NMe_4]^+$ (7d)

A mixture of crude [*closo*-$B_{10}H_9$-1-NH_3]$^-$[NMe_4]$^+$ (**7b[NMe_4]**, 495 mg, 2.40 mmol),[37] 3,3-bis(2-bromoethyl)-1-bromooctane[28] (**11**, 967 mg, 2.4 mmol), dicyclohexyl-18-crown-6 (44.7 mg, 0.12 mmol), anhydrous K_2CO_3 (994 mg, 7.2 mmol) and dry MeCN (25 mL) was stirring under reflux for 7 days under Ar. The suspension was filtered and the solid was washed with MeCN. The filtrate was evaporated and dispersed in an aqueous solution of NMe_4Cl. The brown precipitate was filtered, washed with cold water and dried. The resulting solid was washed with boiling hexanes (50 mL) to yield 889 mg (99% yield) of crude salt **7d[NMe_4]** that was approx. 90% pure based on ^{1}H NMR: ^{1}H NMR (300 MHz, CD_3CN) δ −0.6 to 1.4 (br m, 8H), 0.90 (t, J = 6.9 Hz, 3H), 1.22–1.40 (m, 8H), 1.79 (t, J = 7.9 Hz, 6H), 3.09 (s, 12H), 3.89 (t, J = 7.9 Hz, 6H); ^{1}H NMR (300 MHz, $CDCl_3$) δ 0.5–2.0 (m, 8H), 0.91 (t, J = 6.8 Hz, 3H), 1.25–1.35 (m, 8H), 1.82 (t, J = 7.9 Hz, 6H), 3.28 (s, 12H), 4.01 (t, J = 7.9 Hz, 6H); ^{11}B NMR (64 MHz, CD_3CN) δ −30.0 (d, J = 122 Hz, 4B), −28.3 (d, J = 122 Hz, 4B), −0.6 (d, J = 124 Hz, 1B), 15.3 (br s, 1B); ^{13}C NMR (75 MHz, CD_3CN) major peaks δ 14.2, 23.1, 23.6, 28.5, 30.6 (3C), 33.1, 40.9, 56.1 (4C), 59.1 (3C).

1-Dinitrogen-10-(4-pentyl-1-thiacyclohexyl)-*closo*-decaborate (8a)

Salt **7c[NMe_4]** (6.0 g, 16.5 mmol) was dissolved in a biphasic mixture of water (60 mL) and THF (60 mL) containing $NaNO_2$ (13.0 g, 188 mmol). Acetic acid (8 mL) was slowly added, while the temperature was maintained below 5 °C. The mixture was stirred for 1.5 h during which the THF layer become dark red. Zinc powder (12 g) was added and the mixture was stirred for 1 h. The resulting light yellow mixture was extracted with CH_2Cl_2, the organic layer was dried (Na_2SO_4) and then solvent removed. The yellow solid residue was passed through a silica gel plug (hexane–CH_2Cl_2, 1 : 1) yielding 2.40 g (46% yield based on starting borane **7a[NMe_4]**). An analytical sample was isolated by chromatography (hexanes–CH_2Cl_2, 1 : 1): mp 133 °C decomp.; ^{1}H NMR (400 MHz, $CDCl_3$) major signals δ 0.6–2.0 (br m, 8H), 0.91 (t, J = 6.9 Hz, 3H), 1.26–1.40 (m, 6H), 1.63-1.76 (m, 5H), 2.34 (br d, J = 12.3 Hz, 2H), 3.42 (br t, J = 13.2 Hz, 2H), 3.68 (br d, J = 12.8 Hz, 2H); ^{13}C NMR (100 MHz, $CDCl_3$) major isomer: δ 14.0, 22.5, 26.0, 26.6, 31.0, 31.8, 35.6, 36.0, 36.4, 41.1; ^{11}B NMR (128 MHz, $CDCl_3$) δ −22.0 (d, J = 143 Hz, 4B), −17.3 (d, J = 149 Hz, 4B), −3.9 (s, 1B), 18.6 (s, 1B).

Distinct signals ascribed to **8a-*cis*** isomer present in 25%: ^{1}H NMR δ 0.86–0.89(t), 2.03–2.10 (m), 3.32–3.38 (m) 3.53–3.560 (m); ^{13}C NMR δ 26.2, 33.6, 34.7; ^{11}B NMR δ 16.9.

IR ν_{BH} = 2529 and ν_{NN} = 2223 cm^{-1}; UV (MeCN) λ_{max} (log ε) 253 (4.44); FAB m/z, 313–318 (max at 316, MH^+), 275–290 (max at 283). Anal. calcd for $C_{10}H_{28}B_{10}N_2S$: C, 37.95; H, 8.92; N, 8.85. Found: C, 38.28; H, 9.02; N, 8.81%.

1-Dinitrogen-10-(4-pentyl-1-quinuclidinyl)-*closo*-decaborate (8b)

Crude [*closo*-$B_{10}H_9$-1-(4-pentyl-1-quinuclidinyl)]$^-$[NMe_4]$^+$ (**7d[NMe_4]**, 809 mg, 2.17 mmol) was reacted with 2,4,6-tribromobenzenediazonium $[BF_4]^-$ (989 mg, 2.3 mmol) to yield 348 mg (1.07 mmol, 50% yield based on **6**) of product **8b**. Alternatively, **8b** was obtained in a similar way to the preparation of the sulfonium analogue **8a** by diazotization of anion **7d**: mp 153 °C decomp.; ^{1}H NMR (400 MHz, $CDCl_3$) δ 0.5–2.0 (m, 8H), 0.92 (t, J = 6.8 Hz, 3H), 1.25–1.36 (m, 8H), 1.88 (t, J = 7.9 Hz, 6H), 3.99 (t, J = 8.0 Hz, 6H); ^{11}B NMR (64 MHz, CD_3CN) δ −25.6 (d, J = 129 Hz, 4B), −20.1 (d, J = 142 Hz, 4B), −9.1 (br s, 1B), 30.4 (s, 1B); ^{13}C NMR (75 MHz, CD_3CN) δ 14.2, 23.2, 23.7, 30.3, 33.1, 40.8, 45.3, 59.1; IR (neat) ν_{BH} = 2522 and ν_{NN} = 2211 cm^{-1}; UV (MeCN) λ_{max} (log ε) 255 nm (4.22). Anal. calcd for $C_{12}H_{31}B_{10}N_3$: C, 44.28; H, 9.60; N, 12.91. Found: C, 44.07; H, 9.44; N, 12.83%.

Acknowledgements

This project was supported in part by the NSF grants (DMR-9703002, DMR-0907542, and DMR-1207585). We are grateful to Dr Tom Baker for his generous gift of decaborane. Dr Vladimir Benin, Ryan Nunley, William Tilford, and Erik Brady are thanked for their technical assistance. Dr Donald Stec is acknowledged for his help with NMR experiments.

References

1 V. Vill, *LiqCryst 5.1*, LCI, Hamburg, 2010.
2 H. Kise, Y. Nishisaka, T. Asahara and M. Seno, *Chem. Lett.*, 1978, 1235.
3 B. Ringstrand and P. Kaszynski, *J. Mater. Chem.*, 2010, **20**, 9613.
4 B. Ringstrand and P. Kaszynski, *J. Mater. Chem.*, 2011, **21**, 90.
5 B. Ringstrand, P. Kaszynski, A. Januszko and V. G. Young Jr, *J. Mater. Chem.*, 2009, **19**, 9204.
6 Several mesoionic mesogens have been characterized: B. Künkemeier-Schröder, A.-C. Koch, G. Pelzl and W. Friedrichsen, *Liq. Cryst.*, 1993, **15**, 559; W. L. Chan, W. H. Zhang and Y. S. Szeto, *Mater. Lett.*, 2000, **42**, 280; C. V. Yelamaggad, M. Mathews, U. S. Hiremath, D. S. S. Rao and S. K. Prasad, *Tetrahedron Lett.*, 2005, **46**, 2623.
7 S. Barlow and S. R. Marder, in *Functional Organic Materials. Synthesis, Strategies, and Applications*, ed. T. J. J. Muller and U. H. F. Bunz, Wiley-VCH, Weinheim, 2007, p. 393, and references therein.
8 A. Vöge and D. Gabel, in *Boron Science: New Technologies and Applications*, ed. N. S. Hosmane, CRS Press, New York, 2012, pp. 295–317, and references therein.
9 A. Kaczmarczyk and G. B. Kolski, *J. Phys. Chem.*, 1964, **68**, 1227.
10 J. Aihara, *J. Am. Chem. Soc.*, 1978, **100**, 3339.
11 R. B. King, *Chem. Rev.*, 2001, **101**, 1119.
12 R. D. Dobrott and W. N. Lipscomb, *J. Chem. Phys.*, 1962, **37**, 1779.

13 P. Kaszynski, in *Anisotropic Organic Materials-Approaches to Polar Order*, ed. R. Glaser and P. Kaszynski, ACS Symposium Series, Washington, D. C., 2001, vol. 798, p. 68.
14 R. Zahradnik, V. Balaji and J. Michl, *J. Comput. Chem.*, 1991, **12**, 1147.
15 P. Kaszynski, S. Pakhomov and V. G. Young Jr, *Collect. Czech. Chem. Commun.*, 2002, **67**, 1061.
16 P. Kaszynski, J. Huang, G. S. Jenkins, K. A. Bairamov and D. Lipiak, *Mol. Cryst. Liq. Cryst.*, 1995, **260**, 315.
17 W. H. Knoth, *J. Am. Chem. Soc.*, 1966, **88**, 935.
18 M. F. Hawthorne and F. P. Olsen, *J. Am. Chem. Soc.*, 1965, **87**, 2366.
19 K. M. Harmon, A. B. Harmon and A. A. MacDonald, *J. Am. Chem. Soc.*, 1969, **91**, 323.
20 W. H. Knoth, W. R. Hertler and E. L. Muetterties, *Inorg. Chem.*, 1965, **4**, 280.
21 R. N. Leyden and M. F. Hawthorne, *Inorg. Chem.*, 1975, **14**, 2444.
22 P. Kaszynski and D. Lipiak, in *Materials for Optical Limiting*, ed. R. Crane, K. Lewis, E. V. Stryland and M. Khoshnevisan, Boston, 1995, Vol. MRS, vol. 374, p. 341.
23 J. Zyss, D. S. Chemla and J. F. Nicoud, *J. Chem. Phys.*, 1981, **74**, 4800.
24 A. Miniewicz, A. Samoc, M. Samoc and P. Kaszynski, *J. Appl. Phys.*, 2007, **102**, 033108.
25 M. Komura, H. Nakai and M. Shiro, *J. Chem. Soc., Dalton Trans.*, 1987, 1953.
26 B. Ringstrand, M. Oltmanns, J. A. Batt, A. Jankowiak, R. P. Denicola and P. Kaszynski, *Beilstein J. Org. Chem.*, 2011, **7**, 386.
27 B. Ringstrand, P. Kaszynski, V. G. Young Jr and Z. Janoušek, *Inorg. Chem.*, 2010, **49**, 1166.
28 K. A. Bairamov, A. G. Douglass and P. Kaszynski, *Synth. Commun.*, 1998, **28**, 527.
29 A. G. Douglass, Z. Janousek, P. Kaszynski and V. G. Young Jr, *Inorg. Chem.*, 1998, **37**, 6361.
30 G. H. Schmid and A. W. Wolkoff, *Can. J. Chem.*, 1972, **50**, 1181.
31 Crystal data for **2b** (CCDC no. 875509): $C_{22}H_{47}B_{10}NOS$ triclinic, P-1, a = 9.7645(12) Å, b = 15.716(2) Å, c = 20.148(3) Å, α = 77.516(2)°, β = 83.823(2)°, γ = 86.823(2)°; V = 2948.9(6) Å^3, Z = 4, T = 173(2) K, λ = 0.71073 Å, $R(F^2)$ = 0.0905 or $R_w(F^2)$ = 0.2374 (for 6251 reflections with $I > 2\sigma(I)$). Crystal data for **8a** (CCDC no. 875508): $C_{10}H_{28}N_2S$ monoclinic, $P2_1/n$, a = 10.7989(2) Å, b = 21.0221(4) Å, c = 17.1320(4) Å, β = 99.468(1)°; V = 3836.25(14) Å^3, Z = 8, T = 173(2) K, λ = 0.71073 Å, $R(F^2)$ = 0.0594 or $R_w(F^2)$ = 0.1066 (for 4514 reflections with $I > 2\sigma(I)$). Crystal data for **8b** (CCDC no. 875507): $C_{12}H_{31}N_3$ monoclinic, $P2_1/c$, a = 11.1832(7) Å, b = 11.4422(7) Å, c = 16.2022(10) Å, β = 109.272(1)°; V = 1957.1(2) Å^3, Z = 4, T = 173(2) K, λ = 0.71073 Å, $R(F^2)$ = 0.0578 or $R_w(F^2)$ = 0.1296 (for 2458 reflections with $I > 2\sigma(I)$). For details see ESI.‡
32 L.-L. Ng, B. K. Ng, K. Shelly, C. B. Knobler and M. F. Hawthorne, *Inorg. Chem.*, 1991, **30**, 4278.
33 T. Whelan, P. Brint, T. R. Spalding, W. S. McDonald and D. R. Lloyd, *J. Chem. Soc., Dalton Trans.*, 1982, 2469.
34 H. D. Hall, B. D. Ulrich, R. G. Kultyshev, J. Liu, S. Liu, E. A. Meyers, S. Gréau and S. G. Shore, *Collect. Czech. Chem. Commun.*, 2002, **67**, 1007.
35 A. M. Orlova, I. B. Sivaev, V. L. Lagun, S. B. Katser, K. A. Solntsev and N. T. Kuznetsov, *Russ. J. Coord. Chem.*, 1993, **19**, 129.
36 K. D. Schramm and J. A. Ibers, *Inorg. Chem.*, 1977, **16**, 3287.
37 For details see ESI.‡
38 D. F. Eaton, *Pure Appl. Chem.*, 1988, **60**, 1107.
39 C. Reichardt, *Chem. Rev.*, 1994, **94**, 2319.
40 (*a*) E. V. Lippert, *Z. Elektrochem.*, 1957, **61**, 962; (*b*) N. Mataga, Y. Kaifu and M. Koizumi, *Bull. Chem. Soc. Jpn.*, 1956, **29**, 465.
41 K. Clays and A. Persoons, *Phys. Rev. Lett.*, 1991, **66**, 2980.
42 J. L. Oudar, *J. Chem. Phys.*, 1977, **67**, 446.
43 M. Barzoukas, D. Josse, J. Zyss, P. Gordon and J. O. Morley, *Chem. Phys.*, 1989, **139**, 359.
44 M. J. G. Lesley, A. Woodward, N. J. Taylor, T. B. Marder, I. Cazenobe, I. Ledoux, J. Zyss, A. Thornton, D. W. Bruce and A. K. Kakkar, *Chem. Mater.*, 1998, **10**, 1355.
45 Z. M. Su, X. J. Wang, Z. H. Huang, R. S. Wang, J. K. Feng and J. Z. Sun, *Synth. Met.*, 2001, **119**, 583.
46 K. Clays and A. Persoons, *Rev. Sci. Instrum.*, 1992, **63**, 3285.
47 For the differencebetween HRS and EFISHG methods see K. Clays, E. Hendrickx, T. Verbiest and A. Persoons, *Adv. Mater.*, 1998, **10**, 643.
48 S.-T. Wu, D. Coates and E. Bartmann, *Liq. Cryst.*, 1991, **10**, 635.
49 W. Maier and G. Meier, *Z. Naturforsch., A: Astrophys., Phys. Phys. Chem.*, 1961, **16**, 262 and 470.
50 S. Urban, in *Physical Properties of Liquid Crystals: Nematics*, ed. D. Dunmur, A. Fukuda and G. Luckhurst, IEE, London, 2001, p. 267.
51 W. R. Hertler, W. H. Knoth and E. L. Muetterties, *J. Am. Chem. Soc.*, 1964, **86**, 5434.
52 S. J. Campbell and D. Darwish, *Can. J. Chem.*, 1974, **52**, 2953.
53 D. Darwish and R. L. Tomilson, *J. Am. Chem. Soc.*, 1968, **90**, 5938.
54 S. Toyota, *Rev. Heteroat. Chem.*, 1999, **21**, 139.
55 D. R. Rayner, A. J. Gordon and K. Mislow, *J. Am. Chem. Soc.*, 1968, **90**, 4854.
56 E. L. Eliel, R. L. Willer, A. T. McPhail and K. D. Onan, *J. Am. Chem. Soc.*, 1974, **96**, 3021.
57 E. L. Eliel and R. L. Willer, *J. Am. Chem. Soc.*, 1977, **99**, 1936.
58 H.-J. Schneider and V. Hoppen, *J. Org. Chem.*, 1978, **43**, 3866.
59 J. B. Lambert and R. G. Keske, *J. Org. Chem.*, 1966, **31**, 3429.
60 G. W. Buchanan and V. L. Webb, *Tetrahedron Lett.*, 1983, **24**, 4519.
61 J. B. Lambert, C. E. Mixan and D. S. Bailey, *J. Am. Chem. Soc.*, 1972, **94**, 208.
62 H. Booth and J. R. Everett, *J. Chem. Soc., Perkin Trans. 2*, 1980, 255.
63 H. Herlinger and W. Naegele, *Tetrahedron Lett.*, 1968, 4383.
64 P. K. Claus and F. W. Vierhapper, *J. Chem. Soc., Chem. Commun.*, 1976, 1002.
65 B. Grüner, Z. Janoušek, B. T. King, J. N. Woodford, C. H. Wang, V. Všetečka and J. Michl, *J. Am. Chem. Soc.*, 1999, **121**, 3122 and 2000, **122**, 11274.

66 M. S. Paley and J. M. Harris, *J. Org. Chem.*, 1991, **56**, 568.
67 (*a*) D. G. Allis and J. T. Spencer, *Inorg. Chem.*, 2001, **40**, 3373; (*b*) D. G. Allis and J. T. Spencer, *J. Organomet. Chem.*, 2000, **614–615**, 309.
68 A. D. Becke, *J. Chem. Phys.*, 1993, **98**, 5648.
69 C. Lee, W. Yang and R. G. Parr, *Phys. Rev. B: Condens. Matter Mater. Phys.*, 1988, **37**, 785.
70 M. J. Frisch, *et al.*, *Gaussian 09, Revision C.01*, Gaussian, Inc., Wallingford CT, 2011.
71 J. Pecyna, R. P. Denicola, B. Ringstrand, A. Jankowiak and P. Kaszynski, *Polyhedron*, 2011, **30**, 2505.